Simulations and modeling of light propagation in biological tissue

Towards monitoring oxygen in larger bodies utilizing GASMAS

Emma Hjörneby

17 June 2022

Supervisor: Anna-Lena Sahlberg
Co-supervisor: Emilie Krite Svanberg
Examiner: Mattias Richter

Abstract

The GASMAS technique has previously proven useful for examining and measuring the oxygen concentration in the lungs of preterm infants. GASMAS can distinguish absorption by one gas from the bulk absorption of the surrounding media, and can provide an instant, non-invasive and non-destructive way of examining lungs, and diagnosing dangerous conditions such as pneumothorax. Pneumothorax can be life-threatening if not caught and treated in time, and for patients suffering from lung diseases such as pneumonia or most recently, SARS-COV-2, a monitoring system would be able to alert medical personnel quickly if a lung collapse would occur while patient is treated with mechanical ventilation.

One large obstacle to overcome when scaling up the process, i.e from an infant to an adult, is the amount of light that can be detected, as tissue is a highly scattering media that will distribute the photons over a very large volume, as well as the bulk absorption, which together attenuate the light. This thesis focuses on examining which limits exists for tissue thickness in regards to where the GASMAS technique can be used and to determine the size of body that can be examined using the current best light source and detector placement. This was examined both through simulations of light scattering in tissue using the open-access application *Multi-Scattering*, and through measurements on pork gammon, used as tissue phantoms, using both a tunable diode laser and a Ti:Sa laser. For laser with the output power of 1W, 1.5W and 2W a thickness limit of the phantoms was found, in regards to light-transmission, to be 14 cm (with the presented setup and equipment). This was however not tested using a sweeping tunable laser needed for GASMAS measurements, and must therefore be further investigated to determine the future usability.

Acknowledgements

I would first like to say my warmest thank you to my thesis supervisor, Anna-Lena Sahlberg, Division of Combustion Physics at Lund University, for great support, inspiration and advice.

All laboratory work presented in this thesis have been performed in collaboration with Anna Brandt, who have been a great asset throughout the process and always open for discussing new ideas. Thank you for always bringing a positive mindset, even when things does not go as planned!

A special thanks to Sune Svanberg for always taking the time to help out, even with the smallest of thing. It has always been a pleasure to work with you in the lab!

I would also like to direct my gratitude to my co-supervisor Emilie Krite Svanberg and to Katarina Svanberg, for aiding in the lab and providing guidance on the medical aspects of the work.

A big thank you to Edouard Berrocal and Joakim Jönsson for helping with *Multi-Scattering*, both large and small issues have been solved thanks to you.

Lastly, I would like to thank the team at GPX medical for sharing ideas and guidance, as well as all everyone at the Division of Combustion physics for showing an interest and always helping out when needed. It has been an incredibly educational, fun and (sometimes) stressful spring, but with the help of everyone (named, and un-named) this thesis came together!

Contents

1 Introduction

Patients suffering from a lung collapse are generally diagnosed using chest X-ray, or as an alternative, a lung ultrasound [1, 2] can be used. A downside with both of these techniques is the fact that they only provide momentary information of the current condition. While ultrasound is non-ionizing it is highly user dependant and demands specialized personnel to provide accurate results. A lung collapse, e.g pneumothorax, can be life-threatening if not caught and treated in time, and for patients suffering from lung diseases such as pneumonia or most recently, SARS-COV-2, a monitoring system would be able to alert medical personnel quickly if a lung collapse would occur while patient is treated with mechanical ventilation. A method of continuously monitoring the lungs would provide for faster and more instant care, and a method using non-ionizing radiation would be preferable for both adults and children, considering the risks with frequent exposure to ionizing radiation..

Several previous studies has been done on using GASMAS, GAs in Scattering Media Absorption Spectroscopy, as a tool for examining the gas in lungs [3, 4]. GASMAS can distinguish between the free gas absorption and the absorption by the surrounding media by utilizing the very narrow absorption bands for free gas. This can be utilized to identify the presence of a certain gas [5]. In 2015 Krite Svanberg et. al showed that diode laser spectroscopy could be successfully used to monitor oxygen in the lungs of 29 healthy newborn babies, measuring both oxygen gas (760 nm) and water vapor (937 nm) [3]. Furthermore, in 2019 Krite Svanberg et. al. showed that the same principle could be used on manually ventilated newborn piglets as well, this time using the slightly weaker absorption band for water at 820 nm. With the GASMAS technique it will not only be possible to determine a lung collapse, but to also measure the concentration of oxygen in a certain part of the lung, whilst it being a non-destructive and non-invasive method providing instant feedback [4]. *GPX Medical*[1] is in the process of developing a medical device based on the GASMAS technique for bed side monitoring of the lung function in neonatal infants.

The idea behind this thesis is to further develop the technique and investigate if it is possible to scale up the technique to be used on larger children and adults. The main challenge with larger patient is the high scatter in tissue. The thicker the tissue (i.e when moving from a very small child with no to almost no adipose tissue, to an adult) the more the light will be attenuated when passing through the tissue which decreases the signal. The main idea is therefore to amplify the power of the incident laser radiation, and investigate if enough light can be detected to make it possible to scale up the technique. The use of a tapered amplifier to increase the intensity of the light was suggested by Lin et. al [6] as one method to possibly reach the goal of applying GASMAS on adults.

[1] *GPX Medical is a company based in Lund, Sweden.*

1.1 Goals of the thesis

This thesis aims to determine whether the use of a higher power of the diode laser would render it possible to use the GASMAS-technique for detecting gas in the lungs of larger children and adults, and if possible, determine a limit of the size of the body which GASMAS is applicable for.

This will be done in two parts. Firstly, the photon transport modeling tool *Multi-Scattering* will be used to simulate photons traveling through various thickness of human tissue. Secondly, a GASMAS system, using a tapered amplifier, will be used to investigate if a signal through phantoms can be achieved, and determine if a limit of tissue thickness for light transmission that can be observed. In addition to these measurements a Ti:Sa laser will be used to investigate the same.

1.2 Disposition

This thesis will begin by presenting relevant theory about tissue optics and optical spectroscopy, then continuing on presenting the concept of GASMAS. The thisis has then been divided into two parts. Part I will introduce Monte carlo simulations and the *Multi-scattering* tool as well as present the finished simulations, as well as discussing the accuracy and limitations of the simulations.

Part II will present the experimental arrangements and the result from the three experimental parts performed, where the relation between power and light transmission has been evaluated. First a short evaluation of the current GASMAS system will be presented, leading us in to the light transmission measurements on simple tissue phantoms using the current GASMAS system. This will be followed by a short note about why the measurements using the tapered amplifier have not been performed. Furthermore the results from the measurements done with the the Ti:Sa laser will be presented along with a discussing about their accuracy and reliability, as well as the limitations of the model.

The thesis will conclude with a short summary of all work presented as well as an outlook for the future.

2 Theory

2.1 Tissue optics

The optical properties of biological tissue are crucial for both diagnostic and therapeutic applications of light. The lights ability to penetrate biological tissue, integrate with it's components and escape the tissue again are all key factors for the GASMAS application [7]. In this section some relevant theory surrounding tissue optics will be introduced.

2.1.1 Therapeutic window

The therapeutic window, sometimes also referred to as the optical window, or tissue optical window, for tissue, is a portion of wavelengths in the visible and near-infrared (NIR) region of the wavelength spectrum (ranging from 650 nm to 1350 nm) most suited for use on human tissue, where the combined absorption is minimal and the scattering reduced (when comparing to shorter wavelengths), which makes the tissue relatively transparent [8, 9]. Figure 2.1 shows the absorption for the major tissue components in the human body between 600 nm and 1150 nm. Below 600 nm hemoglobin (Hb) dominates the absorption due to proteins strong absorption of short wavelengths (ultraviolet), and beyond 1400 nm liquid water (which is a large part of the human body) has a high absorption. Other medias to affect the window are melanin, HbO_2 (oxyhemoglobin) and fat [9].

Despite reduced scattering in the therapeutic window, the absorption is not non-existent and light passing through tissue is still heavily attenuated by both absorption and scattering [9].

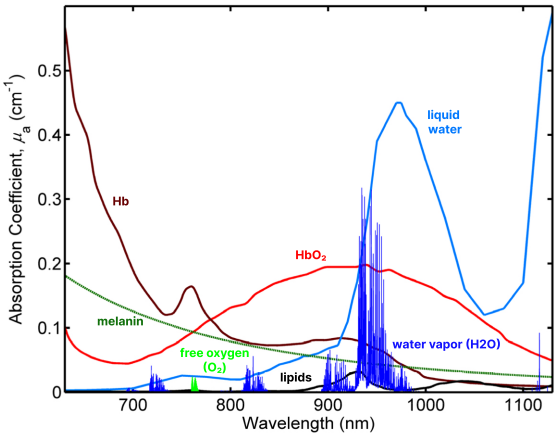

Figure 2.1: The absorption spectra for the major tissue components in the therapeutic window between 600 nm and 1150 nm. Image from [9] with adjustments.

2.1.2 Light attenuation

The attenuation of light passing through a medium is the combined effect of scattering and absorption and is generally controlled by Beer-Lambert law.

$$I = I_0 e^{\mu_{eff} l} \tag{2.1}$$

where I is the transmitted intensity, I_0 is the original intensity and l is the distance travelled, i.e path length and μ_{eff} is the effective attenuation coefficient. For non scattering medias this means the attenuation can be easily derived, but for highly scattering media such as biological tissue, the path length, l, can not be measured and complicates the predicted attenuation. Attenuation will depend on the average path length of all individual photons.

The effective attenuation coefficient can be calculated as 2.2, and shows how it is dependant on both the absorption, μ_a and scattering, μ'_s.

$$\mu_{eff} = \sqrt{3\mu_a(\mu_a + \mu'_s)} \tag{2.2}$$

Scattering

Generally speaking scattering of light occurs when there is an abrupt change in the refractive index in the photon path. For visible and NIR light, scattering in biological tissue is believed to originate mostly from cell nuclei and sub-cellular organelles. [10]

Two types of scattering are often discussed concerning tissue scattering; Rayleigh scattering, which usually refers to scattering by small particles much smaller than the wavelength of light, and Mie scattering, which usually refers to scattering of particles comparable to or larger than the wavelength of light. Per definition Mie scattering is all scattering by a sphere of any size, and Rayleigh scattering refers to the Rayleigh limit of Mie Scattering due to particles much smaller than the wavelength of light.[11] Rayleigh scattering is inversely proportional to the fourth power of wavelength, so that shorter wavelengths (e.g blue light) will scatter more than the longer wavelengths (e.g red light). This is the primary reason for the reduced scattering within the optical window previously mentioned.

Another important factor to consider when discussing scattering is the anisotropy, also referred to as the g-factor, defined as $g = cos\theta$. The g-factor describes the angular distribution of the light scattering, i.e the most likely direction of scattering.

g = 0 indicates a circular distribution, with equal back- as forward scattering

g = 1 indicates purely forward scattering

g = -1 indicates purely backwards scattering

For biological tissue the anisotropy is typically $0.8 > g < 0.98$, which means the light passing through tissue scatter predominately in the forward direction. [8]

Absorption

Absorption is defined as the transfer of electromagnetic light to matter [8]. This occurs when light of a specific energy interacts with an atom or molecule, forcing the molecule from it's initial state (ground state) to a higher energy state (excited state). Due to the very specific amount of energy needed to excite a specific atom or molecule, the absorption spectra is a unique fingerprint for that particular atom or molecule. This means an element can be identified by it's absorption spectra, or that the presence of an element can be determined by observing the absorption over one of the elements absorption lines. [12]

The energy of an atom or molecule is limited to certain specific discrete energy levels. To excite an atom from one energy level to another, the light of the photons need to match the exact energy difference between the levels. This can be explained through Planck's equation. For one specific energy there is precisely one wavelength corresponding to that energy.

$$E_{photon} = h \times \nu \tag{2.3}$$

where ν is the frequency of the light, h is Planck's constant and E is the energy. The frequency is directly related to the wavelength through,

$$\nu = \frac{c}{\lambda} \tag{2.4}$$

where lambda is the wavelength and c is the speed of light.

In figure 2.2 the transition intensities for oxygen between 760 and 762 nm can be seen. These transition intensities is what is also referred to as absorption lines. The sharp absorption lines are unique for gas atoms and molecules. In contrast the bulk media have broad absorption features due to the continuous structure of the energy levels, see figure 2.1.

Note that figure 2.2 only shows a very limited part of the full absorption spectra for oxygen showing only the major transitions within 760 to 762 nm. This image can be compared to 2.1 where the absorption bands for oxygen are shown in relation to other absorbing components in biological tissue.

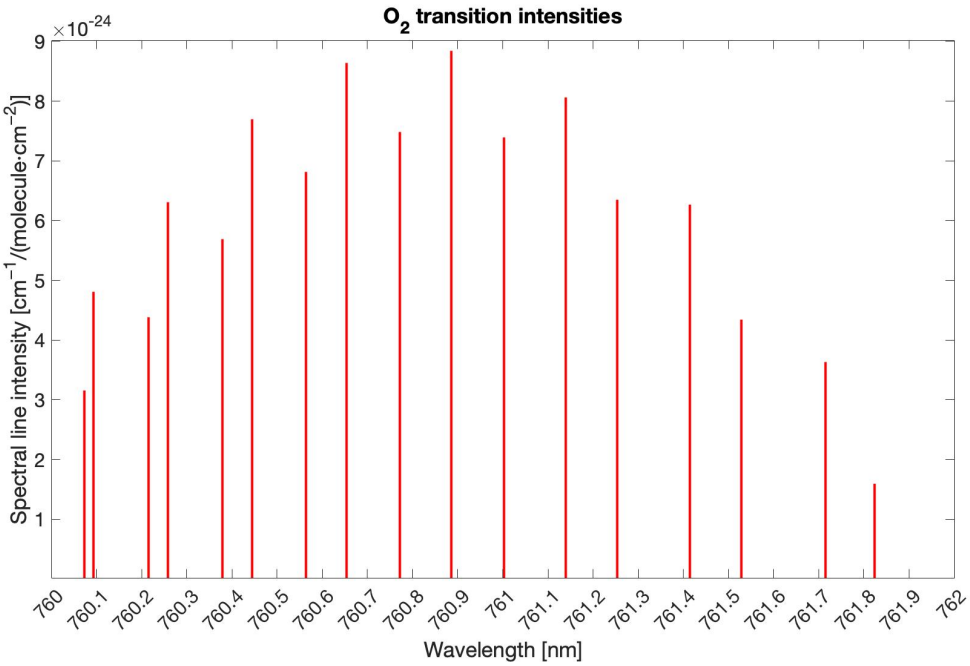

Figure 2.2: Graph showing the transitions intensities for oxygen between 760 nm and 762 nm. Based on data from [13].

Line broadening

The absorption lines, while referred to as lines, are not infinitely thin due to broadening effects spreading them over a larger wavelength range. Two types of broadening can occur, natural broadening and doppler broadening. The Natural broadening is always present, is the same at all wavelengths, and relates to Heisenberg's uncertainty principle which indicates that there is an uncertainty in the energy state of a system. This is due to an uncertainty in the lifetime of the state, as an exited molecule spend very short time in excited state, the exact energy of the state is unknown, and therefore a small interval of wavelengths can excite the atom or molecule, resulting in absorption. Doppler broadening is due to random thermal motion of the atoms or molecules, causing a doppler effect when the light is either moving towards or away compared to the movement of the molecule or atom.[12]

2.1.3 Irradiance

This thesis centers around the idea of a continuous monitoring system, where the skin would be exposed to the laser somewhat continuously. This means that the intensity of the light must be at a level so that the exposure does not heat the skin excessively.

Irradiance is measured in Watt per cm^2, and is defined as the amount of power per area of absorbing surface. By increasing the size of the laser source (e.g by a diffuser) the power can also safely be increased whilst keeping the irradiance constant. To avoid hyperthermic effects, the irradiance should be kept below 150 mW/cm^2, to at maximum generate a 2° temperature increase when exposing the skin. [14, 4] This

would mean that when using a laser output power of 2 W, a diffuser with the minimum area of 13.3 cm^2 (3.65x3.65 cm) should be used. For 1 W 6.7 cm^2 (2.58x2.58 cm) is needed. This is the minimum, and a larger area is preferable to avoid reaching the limit.

2.1.4 Refraction of light

The refractive index of tissue and tissue components is an important part of tissue optics as it determine the light reflection and refraction at the interface between e.g air and tissue, different tissue layers as well as other components within the tissue, resulting in both scattering and the light propagation within the tissue. [15]

The refractive index is a measure of the bending of a ray of light when passing from one medium into another, and is defined either as the ratio between sine of the angle of incidence, i, to the sine of the angle of refraction, r, or as the velocity of light, c, divided by the velocity in the medium, v. [16]

$$n = \frac{\sin i}{\sin r} = \frac{c}{v} \tag{2.5}$$

2.2 Respiratory system

With inhalation the air travels from the nose, through the larynx and down the trachea to reach the lungs. The trachea splits in two bronchi, one leading to each of the lungs, that then branch out into smaller and smaller tubes, giving the lung its tree like structure. The smallest branches are called bronchioles, which lead to tiny air sacs (alveoli). From the alveoli oxygen is transported out into the body by diffusing through the very thin walls of the capillary surrounding the alveoli. As a whole the lungs are divided into sections, or lobes. The right lung is divided into three lobes, while the left is divided into two lobes. Each lobe is then divided into several smaller parts. Each part has its own bronchial, supplying it with air. Each lung is also surrounded by the pleura, which is a double layer of tissue that lines the interior wall of the chest cavity, creating the pleural cavity. [17]

Pneumothorax

A pneumothorax is what in every-day language is referred to as a collapsed lung, and refers to air leaking into the space between the lung and the chest wall (the pleura cavity). This will change the pressure, and push the lung to collapse from the outside, which can worsen ventilation and oxygenation. This can happen to one of the lungs, both, and be a complete or partial collapse of the entire lung, lung lobe or a part of the lung. The most obvious reason for a pneumothorax is external injury to the chest, but it can also occur from certain medical procedures, e.g mechanical ventilation, lung

diseases, and sometimes for no obvious reason, a so called spontaneous pneumothorax occurs. [18]

A pneumothorax is generally diagnosed using a chest X-ray, though both ultrasound and CT are viable options for identification or more detailed images. [1]

Atelectasis

As opposed to pneumathorax, atelectasis occurs when the alveoli within the lung become deflated or filled with alveolar fluid. This is the most common respiratory complication after surgery, but can be caused by chest injuries, lung diseases or fluid in the lungs.

As for pneumothorax, atelectasis can happen to one, or both lungs and be a complete or partial collapse of the entire lung or lobe of the lung. [19] Atelectasis can be diagnosed with a chest X-ray, but to confirm and determine the severity it's usually performed alongside a CT-scan, pulse-oximetry, ultrasound or bronchoscopy.[2]

2.3 GAs in Scattering Media Absorption Spectroscopy (GASMAS)

Gas present in pores or cavities embedded in the tissue will create sharp and element specific gas imprints in the transmitted intensity. The GASMAS-technique utilises the fact that free gas has absorptive imprints up to 10,000 times more narrow than those related to to solid-state material, meaning that free gas can be observed despite being surrounded by highly absorbing solid-state medias, as shown in figure 2.1 and 2.2, and has previously been proven to work for gas evaluation in the lungs of infants [3] and human sinus cavities [20], as well as non-medical application such as wood, pharmaceutical tablets, food packages etc. [5]

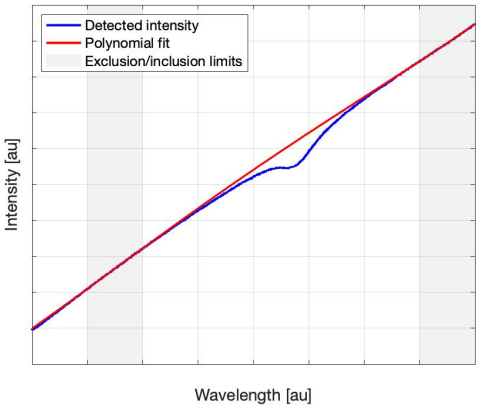

Figure 2.3: Direct absorption spectroscopy where the dip in intensity indicates absorption from oxygen as the wavelength is scanned over a wavelength interval containing one wavelength corresponding to a transition line for oxygen. The grey areas represent the two intervals used for used for lineftting. The fitted line represent the bulk absorption and the difference between the bulk absorption and the detected signal is the intensity loss due to oxygen absorption.

GASMAS is a variety of tunable diode laser spectroscopy (TDLS), utilising the narrow absorption bands of free gas in a very scattering media. In order to retrieve the detected signal shown in 2.3, a tunable laser is scanned over a wavelength interval containing a absorption line for the gas of interest and the light is sent through the sample containing gas. By recording the transmitted light as a function of time, a slightly lower intensity will be recorded as the wavelength matches the wavelength of the absorption line, see 2.3.

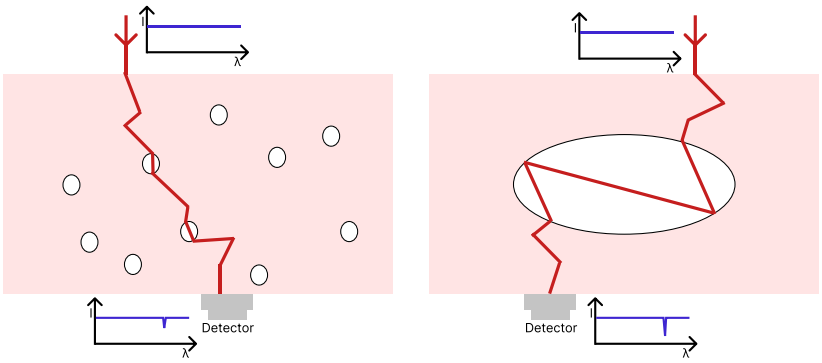

Figure 2.4: Illustration of two different cases where GASMAS can be applied. One possibility is gas located inside small pores in the scattering medium (porous materials) (left), or gas contained within a larger cavity in the scattering medium (right). As light passes the gas, either in pores or in a larger cavity, part of the light will be absorbed due to the gas's specific absorption lines, indicating on the detected signal if the light passed the gas or not.

The bulk absorption (from the surrounding media, in this thesis biological tissue) is constant over all wavelengths within a scan, and is calculated from the detected DAS signal, fig 2.3, where the blue curve is the detected signal, the red curve the bulk

absorption calculated from the grey areas on the graph, and the difference between the two curves is the intensity loss due to free oxygen absorption. The lowering of intensity directly correlates to the path length of the light within free gas according to Beer-Lambert law (eq. 2.1).

In ordinary absorption spectroscopy Beer-Lambert law can be used to calculate the concentration, as the path length of the light between the laser and the detector is known. For purposes of determining the gas concentration, the attenuation coefficient can be separated into the concentration and molar absorptivity. Eq 2.1 can therefore be written as,

$$I = I_0 e^{-\varepsilon c l} \tag{2.6}$$

where ε is the molar absorptivity relating to the specific gas, c is the concentration and l is the path length. With a known average path length and molar absorptivity, the concentration can be calculated.

As mentioned before, the high scattering nature of biological tissue complicates this, as the path length is unknown. All photons traveling through the medium are scattered individually, with some going a short direct path and others a longer path. To determine the average path length of the photons passing through the tissue, the solution is to simultaneously measure the absorptive imprint of another gas with a known concentration. If the concentration is known, eq 2.6 can be used to extract the average path length of the photons through the tissue. Water vapor is a suitable gas for this purpose, since it is present with a known concentration in the lungs. Still, this is only an approximation and adjustments may need to be made.

By normalizing the oxygen signal to the water vapor signal, measured simultaneously, the path length of the oxygen signal can be calculated from the water vapor signal, thus assuming similar path lengths for both signals. This is due to the relative humidity of lungs is close to 100%, as it can be seen as a closed system, and the concentration of water vapor is therefore only determined by the temperature, according to the Arden-Buck equations. [5, 9] With a known concentration for water vapor, the equivalent path length can be calculated. As the path length is assumed to be approximately the same, the oxygen concentration can therefore be calculated.

It is important to note that the relevant path length is only the distance the light have traveled within the free gas, not the full path length of the light through the tissue.

2.3.1 Challenges

- Must be possible to pass enough light through the bulk medium
- Must be possible to distinguish between absorption by the gas and the bulk material
- Quantitative concentration measurements require that the path length is known

2.3.2 Wavelength modulation spectroscopy

Noise can effectively be reduced by modulating the light signal. This is the primary purpose of the Wavelength modulation spectroscopy (WMS). The wavelength of the laser light is modulated at a high frequency, f_{WMS}, with a modulation amplitude, M, and the detected light is evaluated at the modulation frequency or a harmonic of that frequency. The modulation frequency is usually in the order of of kHz, and the modulation amplitude should correspond to the line width of the absorption profile, to avoid line broadening (too large modulation depth) or low signal (too small modulation depth).

The function of the technique can be understood as scanning back and forth over each position of the signal with the frequency f_{WMS}. If the signal is constant, the modulated signal will be as well, as it will experience no difference as it scans over the point with the assigned depth, M. If the sweep passes partly over the absorption line, the modulation signal will experience a change in amplitude, and the outcome will be a sinusoidal with the frequency of f_{WMS} and an amplitude of the difference in amplitude registered. When the sweep completely overlaps the absorption peak, an additional peak will appear within the f_{WMS} sinusoidal, at $2 * f_{WMS}$, as the scan will go from low absorption to the highest and back to low (or from high detected intensity to the lowest detected intensity to high again), before turning back, all within one sweep. From this, the wanted signal can be extracted from within the sinusoidal, rendering the effective 2f-signal. Without absorption, the 2f signal will not appear, and is therefore effectively the oxygen (or other gas) absorption. [21]

2.4 Approximation of a human chest in cross section

By approximating the cross section of a chest as an ellipse, one can get an idea of what thickness off tissue is realistic to be working with. For the following approximations, the major axis (transverse diameter) is assumed to be twice the size of the minor axis (anterior-posterior diameter) which is the normal ratio for an adult chest, see fig 2.5.

The perimeter of an ellipse can be approximated as follows,

$$p \approx \pi\sqrt{2(a^2 + b^2)} \tag{2.7}$$

which gives,

$$b \approx \sqrt{\frac{(\frac{p}{\pi})^2}{10}} \tag{2.8}$$

$$a = 2b \tag{2.9}$$

if the ratio 1:2 is assumed.

This is a very simple approximation, as we here do not consider that the body is actually 3-dimensional, but for size comparison, it can be helpful to consider the

thickness of tissue a truly ballistic photon would be able to travel in transmission. A full term infant have a chest circumference of 31 cm [22], for a small adult, the double should be considered. Using the placements in 2.5a, a truly ballistic photon (not influenced by scattering) would travel ~ 14 cm in an adult with a chest perimeter of 62 cm. For the placement in 2.5b this would be a shorter distance. While this can provide an understanding of the geometries in question, what actually determines the possibility of retrieving successful reading is how much of the light that reaches the lungs before reaching the detector, and to maximize this.

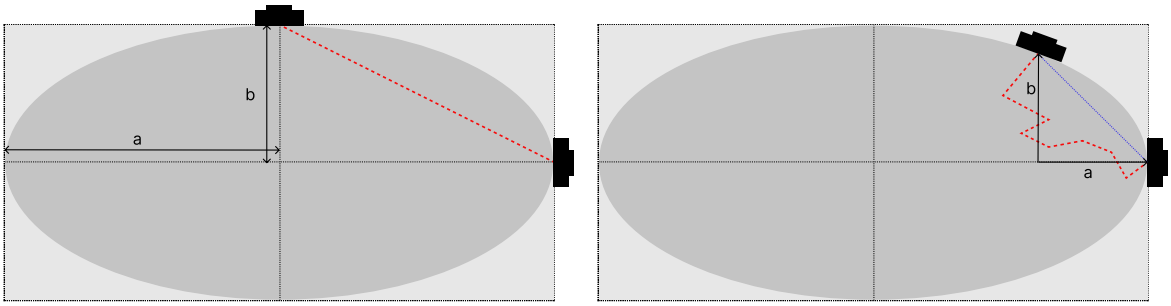

(a) Simple approximation of chest in cross section

(b) A more realistic placement of detector and light source

Figure 2.5: Figures showing a rough approximation of the human chest in cross section. (a) a and b on the major and minor axis of the ellipse corresponding to a and b in equation 2.8, as well as the diagonal distance the light would travel, if it was not affected by scattering. Note that the detector and light source placement of direction in the figure does not correspond to the imagined path, and is only drawn for reference. (b) a more realistic case considering detector placement, as well as a more realistic photon path, but still a very rough approximation.

Placing the light source and detector too close together would result in detected photons that have not passed through the oxygen in the lungs, instead only travel in the upper layers of tissue. This is therefore an important factor to consider. Depending on the depth needed for a viable result. For example if the light do not need to penetrate very deep to reach the lungs (e.g in very small infants with low body fat) the detector and light source can be placed closer together, in contrast, if the light need to penetrate deeper, to close together will mean only surface photons will be detected.

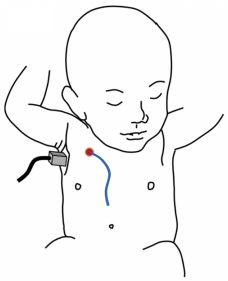

Figure 2.6: Image showing the current detector and light source placement proven to give gas imprints on infant lungs. Image from [23].

In a study from 2013, Lundin et. al considered several different placements of the detector and light source, concluding that an optimal placement for infants is the armpit and the chest [23], as shown in 2.6. Considering a similar placement on an adult the light would have to penetrate deeper to reach the lungs, before turning back up to reach the detector. Despite being a highly scattering medium, tissue is, as mentioned before, primarily forward scattering, which means that the further down in tissue the light travels, the less likely it is to turn back up. It is still reasonable to believe a similar placement would work, as a similar placement on an adult automatically would mean a greater distance between the detector and light source.

3 Part I: Simulations

This chapter gives a short introduction to *Multi-Scattering* and Monte Carlo simulations shortly, as well as present how the simulations were performed, the results and discuss a few limitations to consider.

3.1 Monte Carlo simulations & *Multi-Scattering*

3.1.1 Monte Carlo Simulations

One useful tool to estimate the path of photons within biological tissues is by using Monte Carlo simulations, which is a numerical approach that simulates particles behaviour in a given environment. In this specific case, particles refer to photons in different types of biological tissue.

Monte Carlo simulations rely on three general assumptions [8]

- The photons acts as waves at the site of interaction, and as particles otherwise.
- Photons only interact with the medium, not with each other.
- Unless modified, the simulation does not track polarization and phase such as interface, coherence and nonlinear effects are neglected.

Light scattering is a complex system, but by breaking down the problem into a series of smaller probability calculation, repeating them over and over again, the Monte Carlo algorithm can successfully create an accurate representation. The different possibilities are sampled using randomized numbers and a succession of probability density functions.

3.1.2 Multi-scattering

Multi-scattering [24] is a open access online application for the modeling of light propagation in scattering and absorbing media, developed at the Division of Combustion Physics at Lund University. The software uses the Monte Carlo method to simulate photon transport in media, where the absorption coefficient, μ_α, the scattering coefficient, μ_s, and the anisotropy, g-factor, can be chosen according to the wanted media and simulated according to the Henyey-Greenstein phase function. Monte Carlo simulations relays on random events at large scale becoming predictable and is used to predict the probability of different outcomes when the intervention of random variables is present.

In this thesis the simulations are performed to predict the probability that photons will travel through different types of scattering and absorbing tissues before reach a simulated detector. For each scattering or absorbing event, the free path length (the length travelled before the next interaction event will occur), a new photon weight and a new photon direction is calculated. This is calculated based on the input the user chooses for the medium, and several different mediums can be used to render a 3D (very simple) model. For further reading about how these calculations are executed, see Joakim Jönssons *Multi-scattering Computational light transport in turbid media* [25].

3.1.3 Properties

To be able to perform the simulations, and make them as true to reality as possible a few properties of the different tissues must be known.

Light penetrating the body at the torso will travel through several different types of tissue, e.g skin, adipose tissue, muscle, lung tissue, bone etc. Each of these types of tissue carry certain absorption and scattering properties, many of which lack precise definitions as the properties are much dependant on the subject from which the sample is done on. In table 3.1 values of scattering- and absorption- coefficients for a few relevant tissue types are presented.

Skin

The outer most layer that the light will have to pass to reach the air filled lungs is the skin. The skin can be considered as whole skin, or as the separate layers of the skin (epidermis, dermis and subcutis). Further the epidermis can be divided in to several more layers, but for the purpose of this thesis, only the three main layers will be considered. Skin demonstrates very heterogeneous properties due it's very complex structure, of lipids, glands, blood vessels etc. The values presented in table 3.1 are general values, and can therefore vary depending on mentioned factors. The absorption in epidermis is highly affected by the amount of melanin in the skin, which can be seen in table 3.1. The thickness of the skin varies slightly from person to person and from site to site, but can be said to vary between 0.9 and 2.3 mm over the chest area [26], where the epidermis is about 100-150 μm thick [15].

Adipose tissue

The third layer of skin, the subcutis, is a thin layer of adipose tissue and has a thickness of a few millimeter, up to 6mm, depending on site and individual. Adipose tissue can be found all over the body, and in the area relevant to this thesis, the chest are and the breasts. The absorption in the adipose tissue is predominatly caused by hemoglobin, lipids and water.[15]

Muscle

Further in, the light will reach the muscle tissue. This could be both skeletal muscle, as well as the heart muscle. As with fat, the size of the skeletal muscles are very individual, but an average of 17 healthy individuals show an average thickness of pectoralis major (chest muscle) of 8.35 mm [27].

3.1.4 Choosing parameters for simulations

As noted previously, both the absorbance and scattering coefficients are dependant on tissue type, as well as wavelength. Other things that can effect is the level of hydration, direction of grain (muscle) and if it is tested on living tissue or postmortem. Because of this, in combination with many studies only reporting the absorption coefficient and the reduced scattering coefficient (*Multi-scattering* requires μ_s and g), and that many studies show different results, a combination of several studies have been used to put together the parameters used for the simulations.

When choosing which parameters to use in the simulations the first priority was finding studies reporting the absorption coefficient, the scattering coefficient or the reduced scattering coefficient, and the anisotropy. Secondly the wavelength was considered. For most samples 700 nm, 750 nm, or 800 nm was considered close enough for the coefficients to not differ substantially. Lastly, the found parameter values were compared to other similar values, for example studies reporting absorption and reduced scattering can be compared to studies reporting scattering and anisotropy, if the values has been acquired in the same way. Consequently, values from human tissue has been used, though this was not a significant criteria when choosing parameters to use.

3.2 Method

When choosing the amount of simulated photons a low number was first tried, and then increased until at least one (1) simulated photon reached the simulated detector (mask).

Two types off simulation were done,

- **Basic simulations** where the only medium simulated was lung tissue
- **More realistic simulations** where skin, fat, muscle and lung tissue made up different layers of the medium. These were not based on realistic dimensions, but rather scaled up from smallest to largest, despite this not being the case in real life.

To simulate a detector a circular mask was used with the size 10x10 mm, see figure 3.1b. The detection was done in full transmission, on the opposite side of the light source, located at Y_{min} in figure 3.1a.

Table 3.1: Table presenting scattering and absorption coefficients, and the anistropy for various tissue types that can be found in a torso and chest area. Reference for each tissue type can be found in the table.

Tissue	λ, nm	μ_a, mm^{-1}	μ_s, mm^{-1}	g	Reference
Epidermis (lightly pigmented/medium pigmented/highly pigmented)	700	0.106/0.307/0.711	5.466	0.804	[28]
Caucasian dermis	750	0.103	7.229	0.519	[28]
Caucuasian dermis	761	0.0159	2.05	-	[29]
Human breast (normal glandular tissue)	800	0.055	33.27	0.965	[28]
Human breast (normal adipose tissue)	700	0.081	30.63	0.9749	[28]
Human breast (normal adipose tissue)	800	0.082	31.38	0.976	[28]
Lung epithelum	700	0.11	18.95	0.967	[28]
Lung submucosa	700	0.149	20.50	0.946	[28]
Lung catrilage	700	0.087	24.63	0.965	[28]
Muscle	761	0.072	0.852	-	[29]

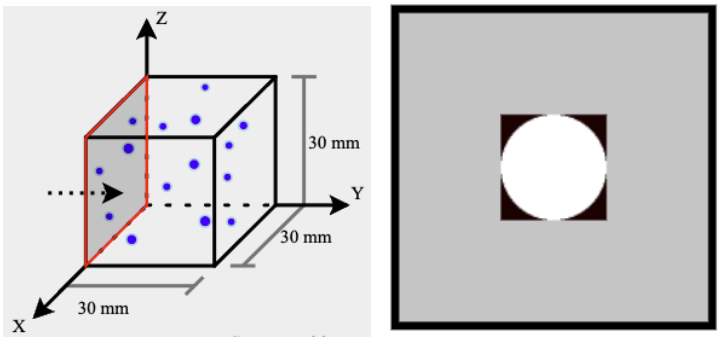

(a) Visualization of the scattering medium

(b) Circular mask used as simulated detector

Figure 3.1: (a) a visualization of the simulated scattering medium, here for 30x30x30 mm large simulation. The light source is placed in the center of the medium at Y_{min}. Detection is done with a circular gate, (b), with the size 10x10 mm, shown on 30x30x30 mm simulation. Detection was done at Y_{max}, in this case 30 mm from the light source.

Due to time and processing constraints, as the application has limited capacity, the simulations are kept both small and relatively uncomplicated. Therefore, the limit of simulated photons was adjusted according to the reached goal. If it was possible to get one (1) simulated photon to reach the detector, this was considered a successful simulation, and the need to simulate more photons was not needed.

This might of course affect the result, as the next time the simulation is run with the same amount of photons the outcome will most likely differ in some way, but this was considered a good enough outcome as one simulation only correspond to one short snippet of a real life situation.

3.2.1 For perspective

The photon energy is dependant on the wavelength as

$$E = \frac{hc}{\lambda} \tag{3.1}$$

where h is Planck's constant, c is the speed of light and λ is the wavelength in meters.

For these simulations 761 nm was used as wavelength, which roughly corresponds to the wavelength used in the experimental part of the thesis. This equals a photon energy of 2.61×10^{-19} joules.

A laser output of 26 mW (as used in measurements presented in section 4.1) equals 26 mJ/s. This corresponds to approximately $9.96 * 10^{16}$ photons per second, or roughly 10^{11} million photons.

Or, looking at it the other way around, 6000 million photons, as used in most of the simulation presented, if seen over one second, would compare to 1.57×10^{-9} mW.

These numbers are still quite unattainable, but explains in some measures the limitations of the simulation application, and further why one detected photon was considered enough. One run of the simulation is therefore only one very small part of what actually would happen in a real environment.

3.3 Results

In this section the results from the simulations are presented, along with a short discussion about the limitations of the application and the simulations.

3.3.1 Basic simulations

The simulations presented in this section are modeled after one medium, lung tissue, and scaled up continuously. The parameters used to simulate lung tissue are,

$$\mu_a = 0.110mm^{-1}, \qquad \mu_s = 18.9mm^{-1} \qquad g = 0.960$$

Lung epithelium was chosen as the medium to simulate, as it scattering and absorption wise lies between lung cartilage and lung submucosa, and was considered a mean. Further information about the parameters used can be found in table 3.1, along values of lung cartilage and lung submucosa, for comparison. For each simulation the general light distribution over the medium, the general photon distribution in cross-section and the photon detected in transmission using a 10x10mm large detector is shown, see figures 3.2 - 3.5. In the 2d images (the general distribution and detected in transmission) all layers are accounted for.

In these simple models there is no change of refracting index, as the whole simulated media is made up out of one material, making the distribution quite symmetrical in the forward direction. The light source is simulated to be 2x2 mm and the simulated detector is 10x10 mm.

The purpose of these simple models were to establish a baseline and an understanding of the scattering process within one media, simplifying it as much as possible, so that other medias and therefore other photon behaviour can be introduced as the models become more and more realistic.

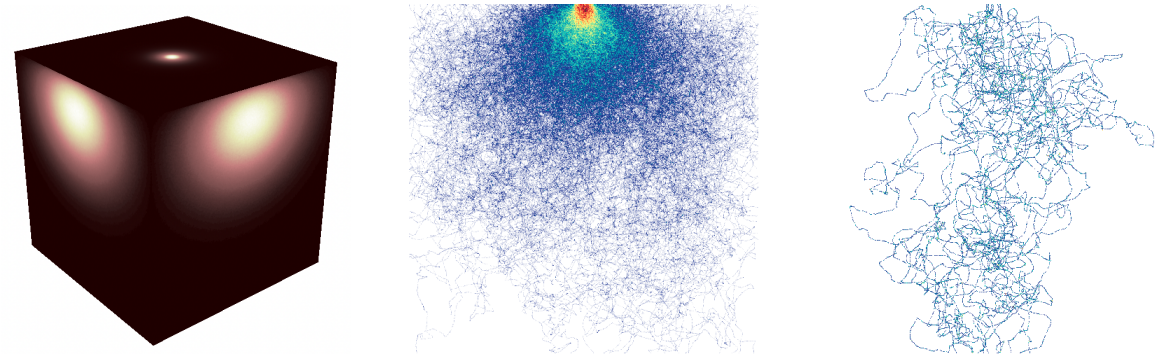

(a) Light distribution **(b)** General distribution **(c)** Detected in transmission

Figure 3.2: Simulation of 12000 million photons in 30x30x30mm lung tissue. (a) shows the light distribution on a 3d model. (b) shows the general distribution in 2d (all layers accounted for), with the light source in top. (c) shows the photon path for those photons reaching a 10x10x10mm detector in full transmission. The colors indicate the concentration of either scattering or absorption in one voxel.

Figure 3.2 shows the results of 12000 million photons simulated in 30x30x30mm lung tissue. In total 1355 photons were registered in figure 3.2b with an average of 734.0 scattering events per photon. 11 photons was registered at the detector in figure 3.2c with an average of 17579 scattering events per photon, resulting in 0,81 % of the photons being detected by the simulated detector.

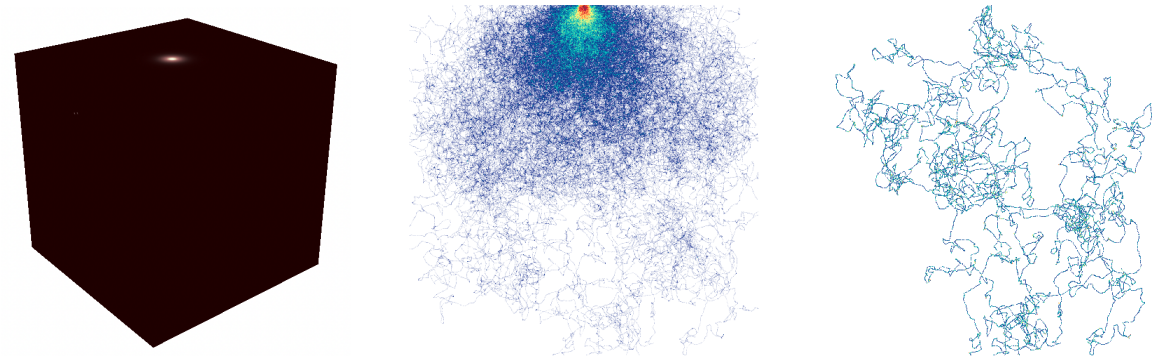

(a) Light distribution **(b)** General distribution **(c)** Detected in transmission

Figure 3.3: Simulation of 12000 million photons in 50x50x50mm lung tissue. (a) shows the light distribution on a 3d model. (b) shows the general distribution in 2d (all layers accounted for), with the light source in top. (c) shows the photon path for those photons reaching a 10x10x10mm detector in full transmission. The colors indicate the concentration of either scattering or absorption in one voxel.

Figure 3.3 shows the result of 12000 million photons simulated in 50x50x50mm lung tissue. In total 765 photons were registered in figure 3.3b with an average of 1303.2 scattering events per photon. 4 photons was registered at the detector in figure 3.3c with an average of 12985.5 scattering events per photon, resulting in 0,052 % of the photons being detected by the simulated detector.

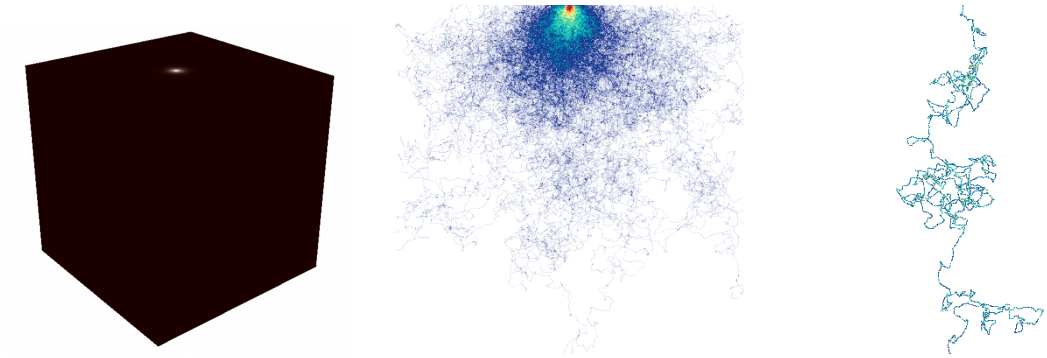

(a) Light distribution **(b)** General distribution **(c)** Detected in transmission

Figure 3.4: Simulation of 16000 million photons in 70x70x70mm lung tissue. (a) shows the light distribution on a 3d model. (b) shows the general distribution in 2d (all layers accounted for), with the light source in top. For this, no photons reached the simulated detector position. The colors indicate the concentration of either scattering or absorption in one voxel.

Figure 3.4 shows the result of 16000 million photons simulated in 70x70x70 mm lung tissue. In total 1150 photons were registered in figure 3.4b with an average of 1432 scattering events per photon. One (1) photon was registered at the detector in figure 3.4c with 17579 scattering events, resulting in 0,087 % of the photons detected by the simulated detector.

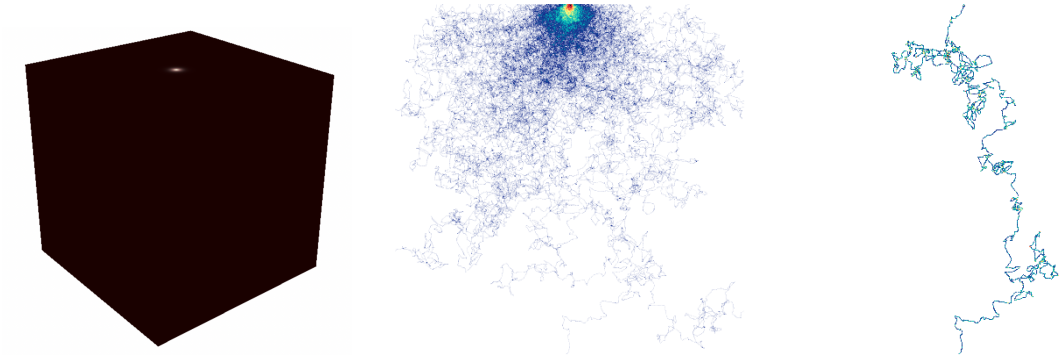

(a) Light distribution **(b)** General distribution **(c)** Detected in transmission

Figure 3.5: Simulation of photon distribution in 90x90x90mm lung tissue using 10000 million photons. (a) shows the light distribution on a 3d model. (b) shows the general distribution in 2d (all layers accounted for), with the light source in top. For this, no photons reached the simulated detector position. The colors indicate the concentration of either scattering or absorption in one voxel.

Figure 3.5 shows the result from simulating 10000 million photons in 90x90x90mm lung tissue. In total 512 photons were registered in figure 3.4b with an average of 1383.4 scattering events per photon. One (1) photon was registered at the detector in figure 3.4c with 18867.0 scattering events. Resulting in 0.19 % of the photons detected by the simulated detector.

While one (1) photon registered at gate was considered a successful simulation, as it enabled *Multi-Scattering* to produce an image of the result. It is not a viable result

concerning the percentage of photons reaching the detector, as it is more of a random event than statistically viable. It should also be noted that in all simulations < 1400 photons was registered, which compared to a real execution would correspond to a very small portion of the photons used.

What instead can be observed from figures 3.2, 3.3, 3.4 and 3.5 is how the photons are distributed over the media. It is possible to visualize how, for each unit of distance the number of photons is cut in half, as the number of scattering and absorption events become fewer and fewer as we travel further down in the simulated tissue. In the same way the photons scattering to the sides become fewer and fewer the further to the side one observes.

What can be considered to gain an understanding of the scattering process and how this will affect the path length is how much the scattering events per photons increases as we travel through a thicker medium. For figures 3.2c and 3.5c the thickness is 3 times as big (from 30 mm to 90 mm) and the average scattering event per photon reaching the detector is increased 5 times.

3.3.2 More realistic simulations

The simulations presented in this section are compromised of layers of different tissue types, and scaled up continuously. The parameters used to simulate the different tissue layers are,

Closest to the light source a layer of epidermis,

$$\mu_a = 0.106mm^{-1}, \qquad \mu_s = 5.466mm^{-1} \qquad g = 0.8$$

Followed by a layer of dermis,

$$\mu_a = 0.103mm^{-1}, \qquad \mu_s = 7.339mm^{-1} \qquad g = 0.51$$

This is followed by a layer of adipose tissue,

$$\mu_a = 0.081mm^{-}1, \qquad \mu_s = 30.63mm^{-1} \qquad g = 0.97$$

And lastly, closest to the detector, a layer of lung tissue,

$$\mu_a = 0.11mm^{-1}, \qquad \mu_s = 18.95mm - 1 \qquad g = 0.96$$

Further information about the parameters used can be found in table 3.1. Epidermis, dermis and adipose tissue were chosen instead of whole skin due to lack of consequent information about the latter. For reference, the scattering- and absorption coefficient for 700 nm and 800 nm for adipose tissue are both present in table 3.1. Values at 700 nm have been used, though important to note that there in no drastic difference. In table 3.1 values for glandular breast tissue is also presented. While it has not been used in the simulations, it is also quite similar to the adipose tissue.

For each simulation the general light distribution over the cube, the general photon distribution in cross-section and the photon detected in transmission using a 10x10mm large detector is shown.

In these more realistic models the refracting index can be seen affecting as the layers are visible in the figure showing the general distribution. This is quite clear when comparing figures 3.2b and 3.6b.

The purpose of these more realistic models is to further build on the simulations presented in section 3.3.1, by adding different tissue types and observing the scattering trough simulations with similar dimensions. This is still a very simple approximation of reality, but could be considered a visualisation of photons traveling from outside the chest into the lungs, travelling through skin, fat and lung tissue. As previously stated, these simulations are not based on realistic dimensions, but rather scaled up from smallest to largest. Despite this not being the case in real life (resulting in e.g disproportional thick skin), it still provides a visualization of scattering amongst different types of tissue.

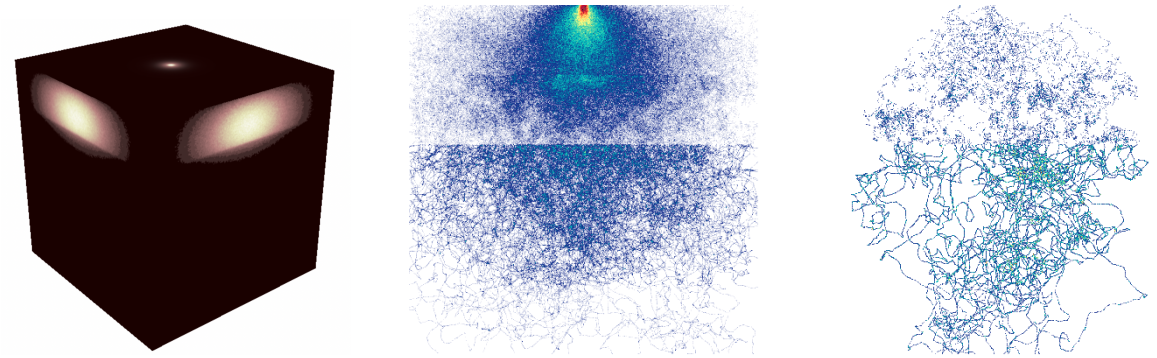

(a) Light distribution **(b)** General distribution **(c)** Detected in transmission

Figure 3.6: Simulation of 6000 million photons simulated in 30x30x30mm tissue, starting with epidermis, adipose tissue and lung tissue. (a) shows the light distribution on a 3d model. (b) shows the general distribution in 2d (all layers accounted for), with the light source in top. (c) shows the photon path for those photons reaching a 10x10x10mm detector in full transmission. The colors indicate the concentration of either scattering or absorption in one voxel.

Figure 3.6 shows 6000 million photons simulated in 30x30x30mm tissue, starting with epidermis, adipose tissue and lung tissue. In total 2591 photons were registered in figure 3.6b with an average of 382 scattering events per photon. 13 photons was registered at the detector in figure 3.6c with an average of 5504.5 scattering events per photon, resulting in 0.50 % of the photons detected by the simulated detector.

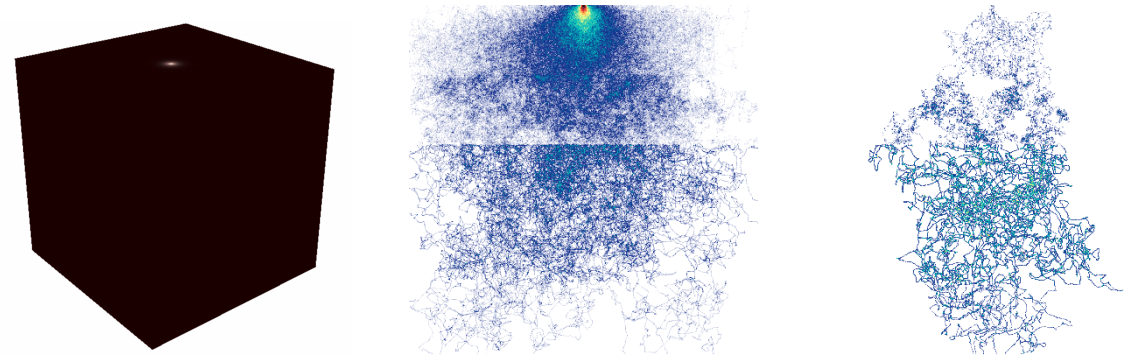

(a) Light distribution **(b)** General distribution **(c)** Detected in transmission

Figure 3.7: Simulation of 6000 million photons simulated in 50x50x50mm tissue, starting with epidermis, adipose tissue and lung tissue. (a) shows the light distribution on a 3d model. (b) shows the general distribution in 2d (all layers accounted for), with the light source in top. (c) shows the photon path for those photons reaching a 10x10x10mm detector in full transmission. The colors indicate the concentration of either scattering or absorption in one voxel.

Figure 3.7 shows 6000 million photons simulated in 50x50x50mm tissue, starting with epidermis, adipose tissue and lung tissue. In total 1457 photons were registered in figure 3.7b with an average of 682.3 scattering events per photon. 7 photons was registered at the detector in figure 3.6c with an average of 17182.6 scattering events per photon, resulting in 0.48 % of the photons detected by the simulated detector.

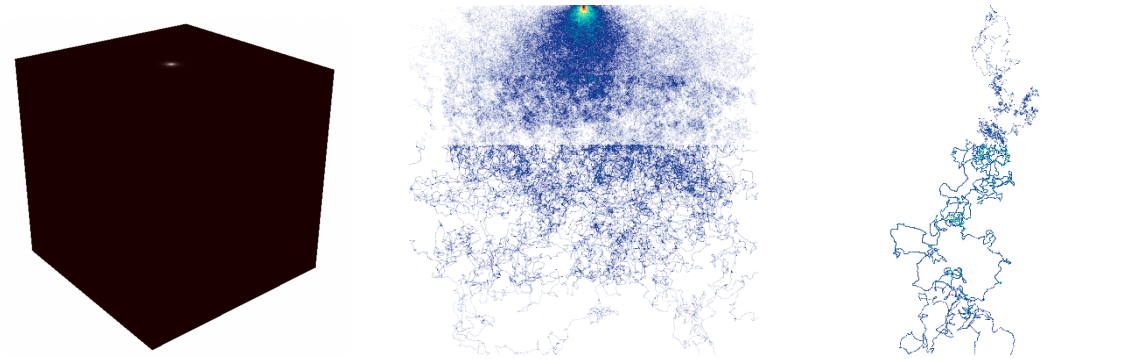

(a) Light distribution **(b)** General distribution **(c)** Detected in transmission

Figure 3.8: Simulation of 6000 million photons simulated in 70x70x70mm tissue, starting with epidermis, adipose tissue and lung tissue. (a) shows the light distribution on a 3d model. (b) shows the general distribution in 2d (all layers accounted for), with the light source in top. (c) shows the photon path for those photons reaching a 10x10x10mm detector in full transmission. The colors indicate the concentration of either scattering or absorption in one voxel.

Figure 3.8 shows 6000 million photons simulated in 70x70x70mm tissue, starting with epidermis, adipose tissue and lung tissue. In total 1124 photons were registered in figure 3.8b with an average of 885.7 scattering events per photon. 2 photons was registered at the detector in figure 3.6c with an average of 15727.5 scattering events per photon, resulting in 0.17 % of the photons detected by the simulated detector.

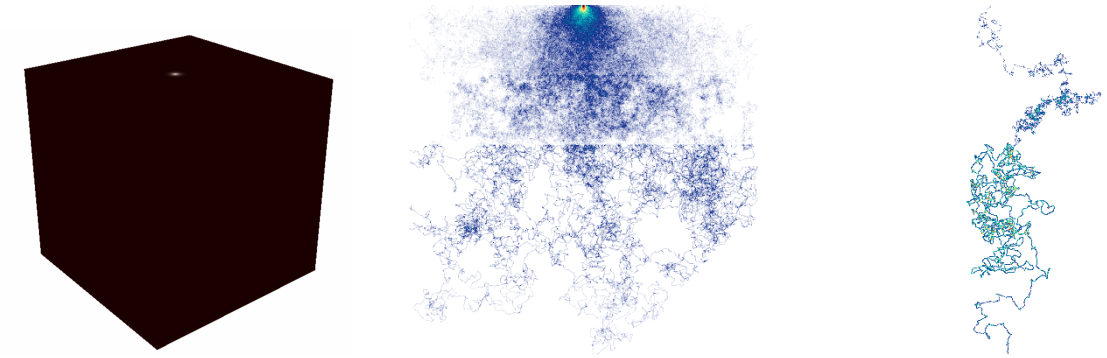

(a) Light distribution **(b)** General distribution **(c)** Detected in transmission

Figure 3.9: Simulation of 6000 million photons simulated in 90x90x90 mm tissue, starting with epidermis, adipose tissue and lung tissue. (a) shows the light distribution on a 3d model. (b) shows the general distribution in 2d (all layers accounted for), with the light source in top. (c) shows the photon path for those photons reaching a 10x10x10mm detector in full transmission. The colors indicate the concentration of either scattering or absorption in one voxel.

Figure 3.9 shows 6000 million photons simulated in 90x90x90 mm tissue, starting with epidermis, adipose tissue and lung tissue. In total 1022 photons were registered in figure 3.9b with an average of 963 scattering events per photon. One (1) photon was registered at the detector in figure 3.6c with 44282.0 scattering events per photon, resulting in 0.097 % of the photons detected by the simulated detector.

The different tissue layers simulated can be seen when observing the general distribution of the photons, creating a visible line of scattering and absorption events as the photons travel from one tissue type to another. The most clear line is between adipose tissue and lung tissue. This is due the the refractive index in the transition between two tissue types causing scattering of the photons.

As previously, too few photons are registered and detected to draw any numerical conclusions from the simulations. What can be observed is that the symmetrical shape of the scattering is still present.

What can be noted as well is the change of scattering event in between the simple model and the more realistic model. For 30 mm (figures 3.2 and 3.6), an increase of 47% was noted, for 50mm (figures 3.3 and 3.7) an increase of 32%. 70 mm (figures 3.4 and 3.8) had a decrease of 10% and 90 mm (figures 3.5 and 3.9) had an increase of 130%. These number can not accurately describe the process, as the number of scattering events are based of of very few photons, but an increase is very reasonable as a change in refractive index causes scattering, and more tissue types would result in more changes in refractive index. Moreover, more scattering events should indicate a longer path length, which increases the overall attenuation.

How the anisotropy affects the scatter can be visualized in all simulations, figures 3.2 - 3.9. All g values used (except for dermis) are predominately forward scattering, resulting in the sides of the models containing fewer photons, compared to middle (if observed in cross-section). This is further confirmed by the detected photons, having a more "direct" path the thicker the model when detected in transmission (compare

figures 3.2 and 3.5. Direct here, indicating only a visually more direct path. As they as mentioned, actually have undergone very many scattering events, most in the forward direction. Observe here that figure 3.2 is 1/3 the size of figure 3.5, and the distance the scatter spreads out over is very similar, alas, the deeper the photons penetrate, the less likely they are to travel to the side. Further, this means the only way to guarantee the photons have passed the lung tissue is by detecting in transmission, as the likelihood of a photon turning back is very small. For the sake of detecting a signal that guaranteed has past through lung tissue, and therefore carrying the information of interest, it is preferable to detect in transmission, as much of the detected photons otherwise will take shortcuts, likely through the dermis, where the back-scatter is as likely as forward scatter.

3.4 Limitation in *Multi-scattering*

Several limitations concerning *Multi-scattering* were acknowledged when creating more life like models of the human body.

- The number of photons registered. The more complex model (more voxels, or larger voxel size) the less photons were registered, resulting in a limitation of either the size of the model or the number of registered photons.
- With few registered and/or detected photons, no numerical conclusions can be drawn from the information. Trends, such as generally more scattering events or longer path length, can be assumed but not proven.
- Due to scaling limitations (a maximum of 20x20 voxels) it was impossible to create large scale models where the measurements were realistic, e.g it was impossible to create a model with 2 mm thick skin, while wanting to generate a model larger than 40x40 mm.

4 Part II: Phantom measurements

This chapter will cover the experimental work performed on tissue-phantoms, with the purpose of evaluating the limit of light detection in transmission.

4.1 GASMAS measurements on a wild boar lung

To enable a comparison between the system with, and without the tapered amplifier and the amplified power of the laser, a series of measurements were first done on a wild boar lung using the existing GASMAS setup. The purpose was to establish a baseline for the current transmission limit of the system. The measurements were performed by filling the lung with air respectively nitrogen, so that the system set up could be evaluated. An oxygen signal should only be present when the lung is filled with air, and if detected when lung is filled with nitrogen, the light passes through air (i.e oxygen) outside of the sample.

4.1.1 Simple GASMAS setup

The simple GASMAS setup consists of a tunable diode laser controlled by a temperature controller and a current controller. By changing the current slightly up or down a wavelength sweep is accomplished, as the current and temperature of the laser determines the wavelength of the laser. The current is controlled by a pre-written LabVIEW interface, developed for GASMAS measurements [23].

The detector is connected to an amplifier, that at maximum can amplify the detected signal up to 10^7 times. A schematic of the setup can be seen below in figure 4.1

Laser diode

To generate the NIR laser light needed for GASMAS measurements of oxygen a tunable 760 nm distributed feedback laser (Eagleyard Photonics, EYP-DFB-0760-00040-1500-BFW01-0002),was used with a $P_{opt} = 40$ mW. In reality, $P_{max} \approx 35$ mW, due to our need for a very specific wavelength. The laser was mounted on a butterfly laser diode mount (ThorLabs, LM14S2) and connected to a laser diode controller (ThorLabs, LDC205C) and a temperature controller (ThorLabs, TED200C). From the diode laser output a fibre was connected, rendering a final output of $P \approx 26$ mW after the fibre.

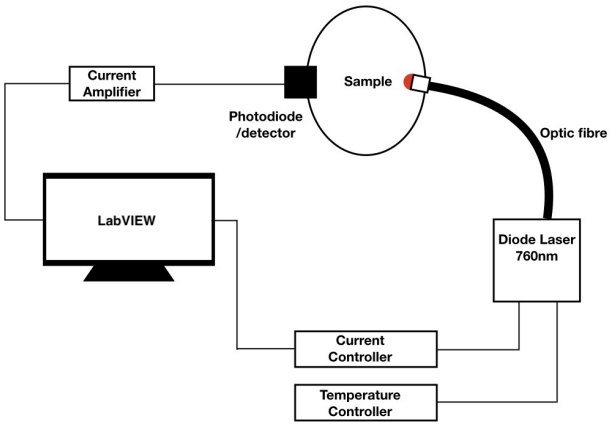

Figure 4.1: Schematic diagram of the setup used, also called "simple GASMAS setup". The diode laser is controlled by a temperature controller and a current controller. The current is controlled by a computer to enable the sweeping function. The laser light is fed through an optic fibre to avoid light travelling through air before reaching the sample. The detector is connected to a amplifier.

Detection

For detection a 10x10 mm Si PIN photodiode (Hamamatsu, S3590-01) connected to a variable gain high speed current detector (Femto, DHPCA-100) was used. To block unwanted wavelengths from reaching the detector (and avoid needing to black out the area completely) a bandpass filter was used in front of the photodiode, with a center wavelength of 760 nm ± 2 nm, and the full width at half maximum (FWHM) is 10 nm ± 2 nm (ThorLabs, FB760-10).

Wave meter

To maximize the detection capability, it is important to choose a line with the highest transition intensity (as depicted in figure 2.2). To determine the correct absorption line, a high precision wave meter (High Finesse, WS5) was used to measure the exact laser wavelength. This was done simultaneously with direct absorption spectroscopy measurements, to compare where the highest absorption signal could be found.

4.1.2 Method

To simulate the conditions of a working lung, the boar lung was flushed with air respectively nitrogen by connecting it using a tracheal tube, keeping a steady airflow to keep the lung inflated. The lung had some minor leakage, which was the reason behind keeping the air flow steady throughout the measurements.

Each GASMAS measurement was acquired as an average of 1000 sweeps over the absorption line, to ensure random noise was not predominant in the measurements.

WMS was applied during the measurements to enhance the sensitivity. Several different detector and optic fiber placements were tested a placement where a signal could be detected was found. Figure 4.2 shows the detector and optic fibre placement in relation to the lung.

At this point two main things were of interest. To test the sensitivity of the system by acquiring an oxygen signal when the lung is filled with air, and the opposite when the lung is filled with nitrogen, in order to determine that the oxygen measured comes from a GASMAS signal inside the lung and not from direct absorption of light passing through air outside the lung.

Figure 4.2: Wild boar lung filled with air with the optic fibre and detector visible, show how the transmission measurements were performed. To prevent the optic fibre from poking a hole in the lung tissue, the lungs was held in place during the measurements.

4.1.3 Results

Figure 4.3a shows 3 measurements from the lung filled with air, and figure 4.3b shows 2 measurements from the lung filled with nitrogen. The signals are collected from light transmission through 5 cm wild boar lung. Each measurement is averaged over 1000 sweeps on the diode laser. In 4.3a the peaks indicating that oxygen is present are clearly visible with a SNR > 6. In figure 4.3b it is still possible to discern the oxygen peaks in the signal, though with a much lower SNR < 3. Ideally an oxygen signal should not be present when the lung is filled with nitrogen. This is most likely due to a non air-sealed system, where the light travel a short distance in air before entering the optical fiber used to direct the light. It is also possible that there were small pockets of air left in the lung despite flushing with nitrogen for several minutes. Still, these two measurements indicate that the setup is functional for the GASMAS measurements, and will work as a base when further developing the system with a TPA.

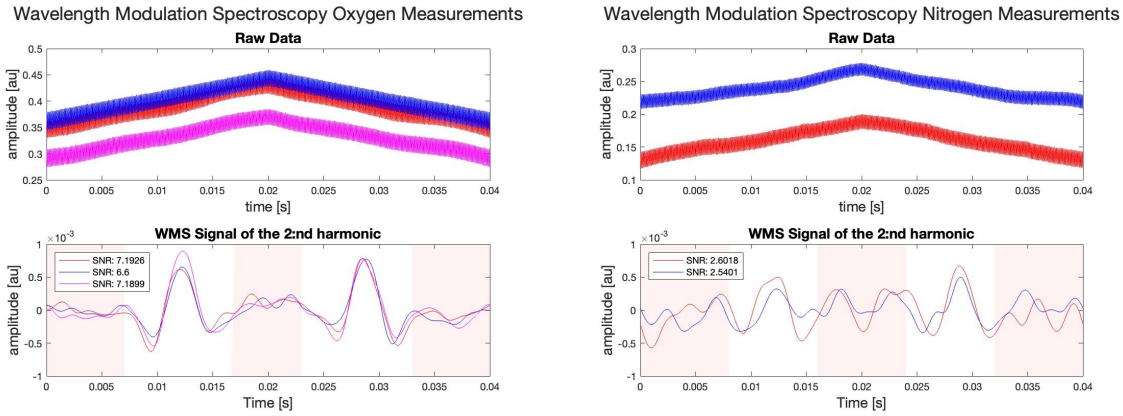

(a) Lung filled with air (% O_2)

(b) Lung filled with nitrogen (N_2)

Figure 4.3: (a) The raw signal as well as the WMS signal of the 2:nd harmonic for measurements on a wild boar lung filled with air (% O_2) (5 cm in transmission). (b) The raw signal as well as the WMS signal of the second harmonic for measurements on a wild boar lung filled with nitrogen (N_2) (5 cm in transmission). In (a) the two oxygen peaks are visible for all three measurements, with a signal-to-noise ratio > 6.6. In (b) the signal to noise ratio < 3, though it is still possible to discern the oxygen peaks in the signal, this is possibly due to not using a fully air sealed system, as well as residue from the air still present in the lung.

4.1.4 Conclusions for further measurements

It was established that for future measurements the whole setup needed to be confined from air, e.g by placing it in a air-sealed box flushed with nitrogen, to prevent light absorption by air anywhere outside the sample. It is important that the photons do not interact with oxygen in unwanted places, as this affects the true result. It was also noted that a more through flushing of the lung should be done when switching between air and nitrogen, so that no residue air is present when filling the lung with nitrogen, for more accurate readings.

One source of noise during GASMAS measurements is the problem of interference fringes. Fringes occur due to partial reflections in parallel optical surfaces, and are a common problem in setups using optical fibers. The periodic interference causes constructive and destructive interference at different wavelengths, leading to a periodic light intensity modulation that can obscure the real spectroscopic signals. In order to avoid the noise caused by unwanted interference fringes, a mechanical vibrator can be attached to the optic fiber. The vibration randomizes the period of the interference fringes, which causes them to cancel each other out when averaging the signals over many wavelength sweeps.

4.2 Diode laser light transmission measurements

The purpose of these measurements was to investigate the relationship between transmission and intensity for different tissue thicknesses. To enable to results from the GASMAS system to be compared to the results from the measurements done with the Ti:Sa laser, they were performed off-line (scan not overlapping an absorption line for oxygen). As previously, one measurement as acquired as an average of 1000 sweeps. The measurement series was started on 5 cm, based on the lung measurements mentioned in section 4.1.3. Powers between 5 mW and 45 mW was used.

The measurements were done without absorption of oxygen for three reasons:

- Limitation in the output power of the diode laser when being on-line
- No optical fiber could be used due to power loss
- For an accurate comparison to the Ti:Sa measurements, as they were performed without oxygen absorption.

As mentioned in section 4.1.1 there is a loss of power when using an optical fiber, and to enable the higher outputs for these measurements ($>$ 30 mW), no fiber was used. This would therefore mean the light would travel in air before reaching the target, and if measurements were done on an absorption line, the reading still would not be accurate in comparison to the ideal conditions.

Pork gammon was chosen as phantom medium as it is mostly muscle and fat, as would be the dominant tissue types in the chest area (excluding lung tissue and skin). The shape also makes it easy to determine the size, and divide into symmetrical pieces. While still being biological tissue, this is to be considered a very simple phantom as it is quite heterogeneous, and lacking for example blood, while most likely containing an disproportional amount of water.

To perform each measurement the power output was chosen and then each thickness was examined for that power. This was considered the easiest way to perform the different measurements, and while it meant the detector placement might change between each thickness of the phantom, it was not possible to avoid.

4.2.1 Results

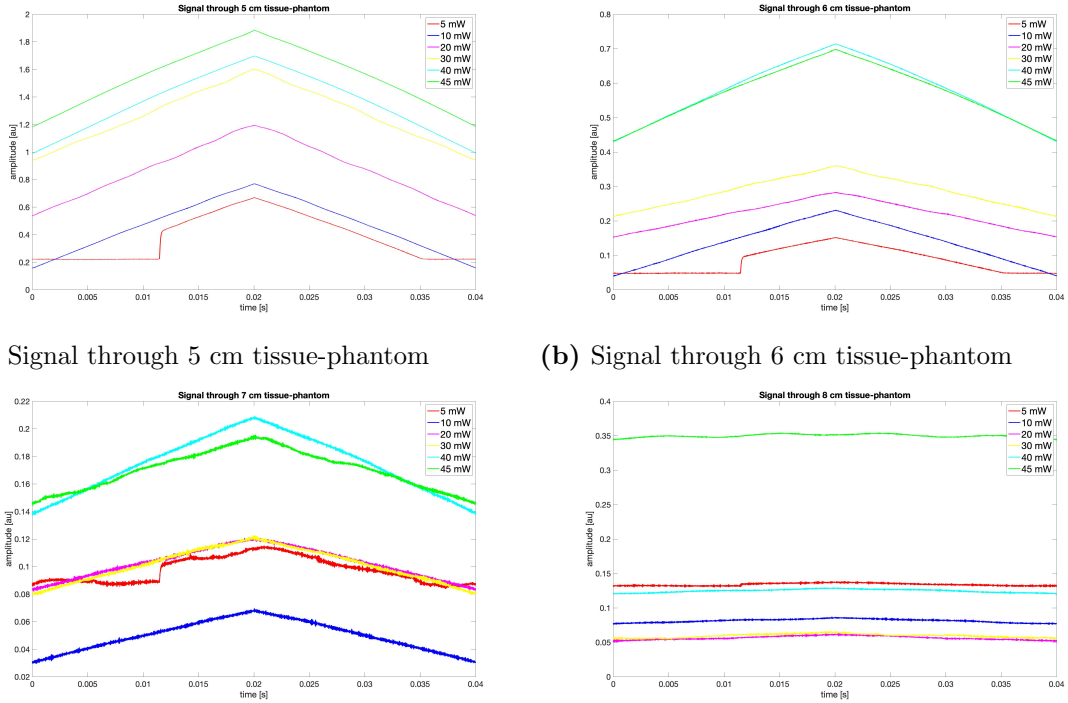

(a) Signal through 5 cm tissue-phantom

(b) Signal through 6 cm tissue-phantom

(c) Signal through 7 cm tissue-phantom

(d) Signal through 8 cm tissue-phantom

Figure 4.4: Using the the simple GASMAS-setup the measurements presented were acquired. The wanted result is the thin triangular shape than can be seen for 40 mW and 45 mW in (a) and (b). All powers are unable to penetrate 8 cm, as can be seen in (d). Here they all lack the triangular shape, as well as showing significant noise compared to (a).

Figure 4.4 shows the transmission of light through different thickness of tissue using the simple GASMAS setup. The reason the sweep is not perfectly triangular for 5 mW is due to the laser in use not sweeping accurately at low powers, as clearly visible in figures 4.4a and 4.4b. This can also be seen in figures 4.4c and 4.4d, while not as clear due to other noise or low signal in general.

For these measurements, only a visual comparison between the results have been done. Due to being off-line there is no oxygen absorption in the signals that can be evaluated. The visual in the first thing determined when searching for a good signal using the simple GASMAS setup, as direct feedback is given by the LabVIEW interface in use. To be able to acquire a good result the signal should look like in figures 4.4a, 4.4b or 4.4c excluding 5 mW (red) and 45 mW (green). It is highly possible that wave-modulation (WMS) would eliminate the noise seen in 5 mW and 45 mW.

These measurements indicate that while examining these small changes in powers, no change can be observed in the detected signals. As 40 mW is detected fine through 7 cm tissue phantom and 45 mW is not, it is plausible this indicates faulty measurements, or simply that the change is to small and that it is still too random if a viable measurements can be acquired. A third plausible reason is the laser output power

being unstable, as it has been observed to drift in power while running the measurements. Though it should be said that no change indicating this was observed during the measurements.

Here it is important to note that there is up to $\pm$ 0.5 cm deviation in the phantom size, which in this case can affect the measurements quite significantly, and that for powers as low as those discussed here, smaller changes should perhaps have been observed to gain a true understanding of how the detected signals viability relates to the laser power and the thickness of the phantom. Each measurement is averaged over 1000 scans, which is needed to eliminate random noise, and to acquire a viable signal. In addition, the effect was set, and then each thickness was measured on that effect, meaning that the detector was moved between each measurement, which gives each measurement different conditions.

4.3 Tapered amplifier GASMAS-system

The original proposal for this thesis was a tapered amplifier (TPA) to enhance the power from the existing diode laser. This setup is based on the simple GASMAS setup, with a few additions, and would enable direct comparisons between different powers when using GASMAS. The TPA has a amplification gain of 15 dB, that, under the right circumstances provide a power of 1 W.

Measurements using the TPA has unfortunately not been possible, as the system is not yet finalized. Instead a Ti:Sa-laser was used to investigate the transmission of higher laser powers through tissue, at a wavelength close to 761 nm. This system differs a bit from a GASMAS-system, but will still present an idea of what results could be expected once the TPA is in use.

4.4 Ti:sapphire light transmission measurements

To examine how a higher power would affect the detection in transmission a tunable Ti:Sa laser system set to 759.6 nm was used. The laser is M Squared SolsTis platform, and is a continuous-wave Ti:Sapphire laser pumped by a Nd:YAG laser. The laser uses a half wave plate to adjust the polarization of the light, resulting in an adjustable power output, from 100mW to 2W.

A chopper wheel placed in the laser beam path was used to simulate the sweeps in the GASMAS system, and to provide a state of signal respectively no signal, as the wheel blocks and unblocks the laser rotating with a frequency of 8 Hz.

By using the same detector and detector amplifier as previously (see section 4.1.1) the light transmission measurements can be compared.

In figure 4.5 8, 12 and 15 cm pork gammon used in the measurements with the Ti:Sa laser. The laser input and detector placement is roughly along the same placement

as the ruler to account for differences and asymmetry in the pieces. A error of ±0.5 cm should be considered in the thickness, though the placement of the phantom was considered to minimize this.

(a) 8 cm pork gammon **(b)** 12 cm pork gammon **(c)** 15 cm pork gammon

Figure 4.5: 8, 12 and 15 cm pork gammon used in the measurements with the Ti:Sa laser. The laser input and detector placement is roughly along the same placement as the ruler to account for differences and asymmetry in the pieces. A error of ±0.5 cm should be considered.

About the data

Data collected from 11 cm and up have been measured with a 10x higher resolution, which is why more data points was collected over the same time. This is the reason for the visual difference between the raw signal in figures 4.6a and 4.6d.

Data collected from 14 cm and up have been measured with the phantom covered by aluminium foil to protect from scattered light in the room from the laser. At low power (below 1 W) this is not an issue, and was not considered to affect the measurements significantly before the thicker phantoms where the signals get very small.

Each measurement for one phantom thickness was done without moving the phantom or detector, only adjusting the power of the laser. This means that for one power the detector has been moved between each measurement.

4.4.1 Results

The following section shows the results from the measurements performed with the Ti:Sa-laser on pork gammon. Presented in figure 4.6 is the raw measured signal as well as the averaged signal, which is considered the true signal compared to the noise. The high intensity in the signal corresponds to light transmitted through the sample, while the low intensity signal occurs when the chopper wheel is blocking the laser light from entering the sample. The offset of the plots have been adjusted for, for easier comparison between them, therefore negative values are present.

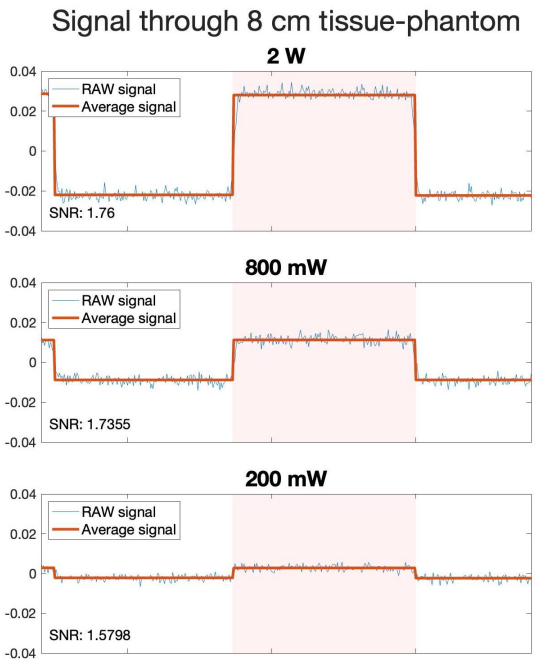

(a) Signal detected in transmission through 8 cm gammon

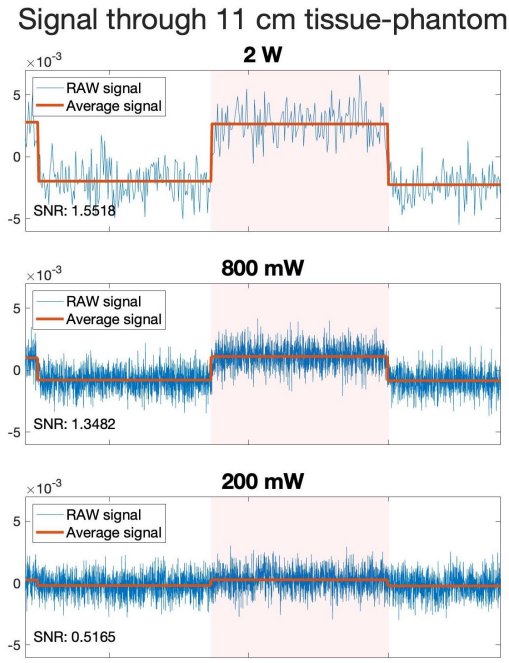

(b) Signal detected in transmission through 11 cm gammon

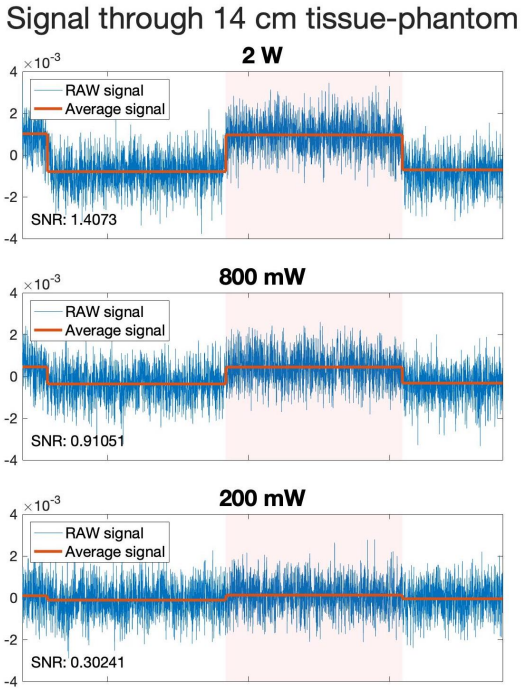

(c) Signal detected in transmission through 14 cm gammon

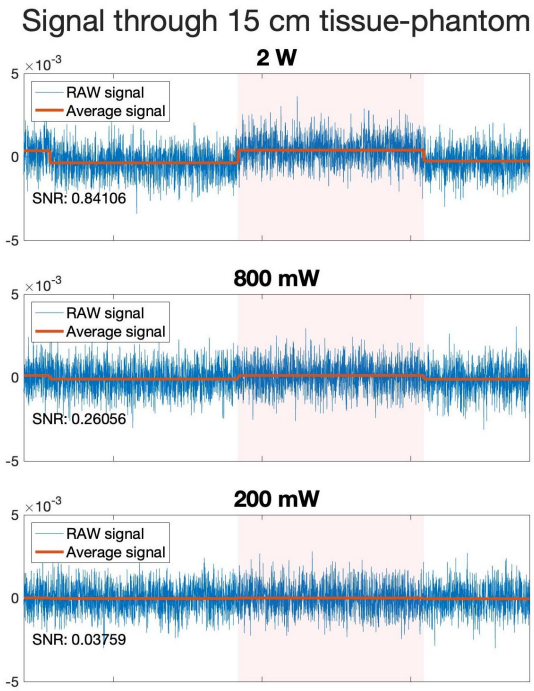

(d) Signal detected in transmission through 15 cm gammon

Figure 4.6: (a) the signal through 8 cm of tissue phantom for 2 W, 800 mW and 200 mW. (b) the signal through 11 cm of tissue phantom for 2 W, 800 mW and 200 mW. (c) the signal through 14 cm of tissue phantom for 2 W, 800 mW and 200 mW. (d) the signal through 15 cm of tissue phantom for 2 W, 800 mW and 200 mW. In blue the raw signal is shown, and in red the average is shown (considered the actual signal). For each graph the signal-to-noise ratio is present. Marked in pink is the area of which the RMS value of the noise (raw signal) has been calculated to calculate the SNR value of each graph.

Note the scale difference between the data presented in figures 4.6a-d when comparing them. All three plots in each figure are the same scale.

Marked in pink is the area within the root mean square (RMS) value of the noise (raw signal) has been calculated. Here it has been assumed the noise behaves similar at signal and at no signal, which can be visually confirmed by observing the graphs.

The signal-to-noise ratio is defined as as the ratio between the difference between signal and background, and the RMS values of the noise over the signal.

Observing the SNR values in figure 4.6 the following can be concluded

- SNR > 1.7 has no overlap of noise, as can be seen in both for 2 W and 800 mW in figure 4.6a
- SNR ≈ 1.5 has some overlap of the noise, but a clear signal can still be depicted, as can be seen in 200 mW in figure 4.6a, 2 W in figure 4.6b or 2 W in figure 4.6c
- SNR < 1 has large overlap of noise, and while a signal can still be depicted for e.g 800 mW in figure 4.6c or 2 W in figure 4.6d, the overlap of noise is considered to be too large.

SNR curve fitting

Figure 4.7 show the SNR values for all phantom thicknesses for 2 W respectively 200 mW plotted in relation to the phantom thickness. The values have been fitted using an exponential curve, also shown in the graph. The points marked with a red circle has been excluded from the fit due to them deviating from the trend.

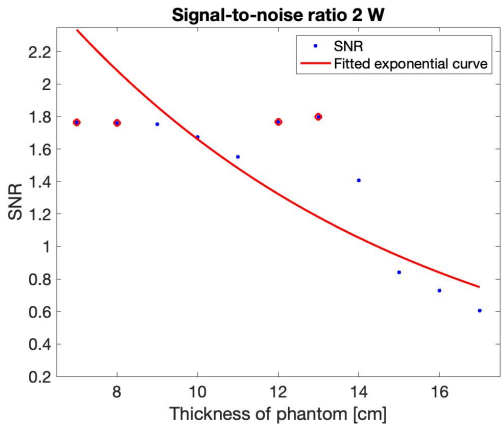

(a) Signal to noise ratio as a function of phantom thickness for 2 W

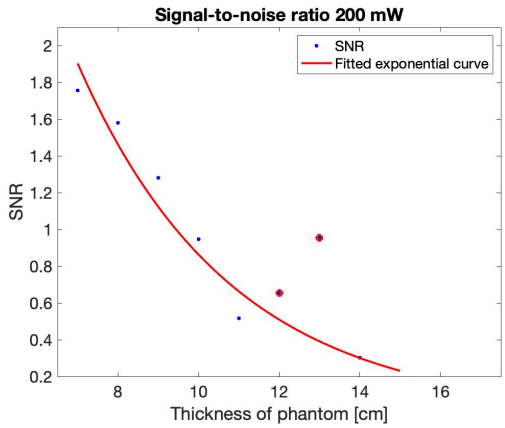

(b) Signal to noise ratio as a function of phantom thickness for 200 mW

Figure 4.7: (a) showing the fitted curve as well as the values of signal-to-noise ratio for 2W for 7-17 cm for 2 W. (b) showing the fitted curve as well as the values of the signal-to-noise ratio for 7-15 cm for 200 mW. The SNR value at 12 cm and 13 cm has been excluded from both fittings, but is shown in the graphs, marked with a red circle.

Figure 4.8 shows the fitted curves for all powers from 100 mW to 2 W. For each powers SNR values at 12 and 13 cm have been excluded from the fitting. For 2W SNR values at 7 and 8 cm have also been excluded. All calculated SNR values can be seen in table 4.1, where all values excluded from the fitting process are marked in yellow and SNR values < 1 are marked in red, for an easy overview.

For all fittings except, 100 mW, in figure 4.8 the exponential fitting were done excluding the SNR value at 12 and 13 cm. In figure 4.7 and table 4.1, it is possible to see that the SNR value at 12 an 13 cm is consistently higher than previous values and do not follow the trend of decreasing when the phantom thickness is increased. This is true for the SNR value at 12 and 13 cm for all powers. There is a high likelihood this is due to either faulty detector placement, were a higher amount of stray light (light scattered in the room finding it's way back to the detector) where able to reach the detector, or that the stray light in the room affected more at this stage. From 14 cm and onward, the phantom was covered with aluminium foil to avoid this.

For 2 W the SNR values at 7 and 8 cm have also been excluded from the fitting, but are plotted in figure 4.7a. The SNR value is seemingly unchanged for the three first SNR values for 2 W. This indicates a threshold where the noise is low enough in comparison to the signal, and that the signal is seemingly unchanged. It is possible that the detector was saturated at these points, due to high power and low thickness of the phantom leading to high levels of light transmission.

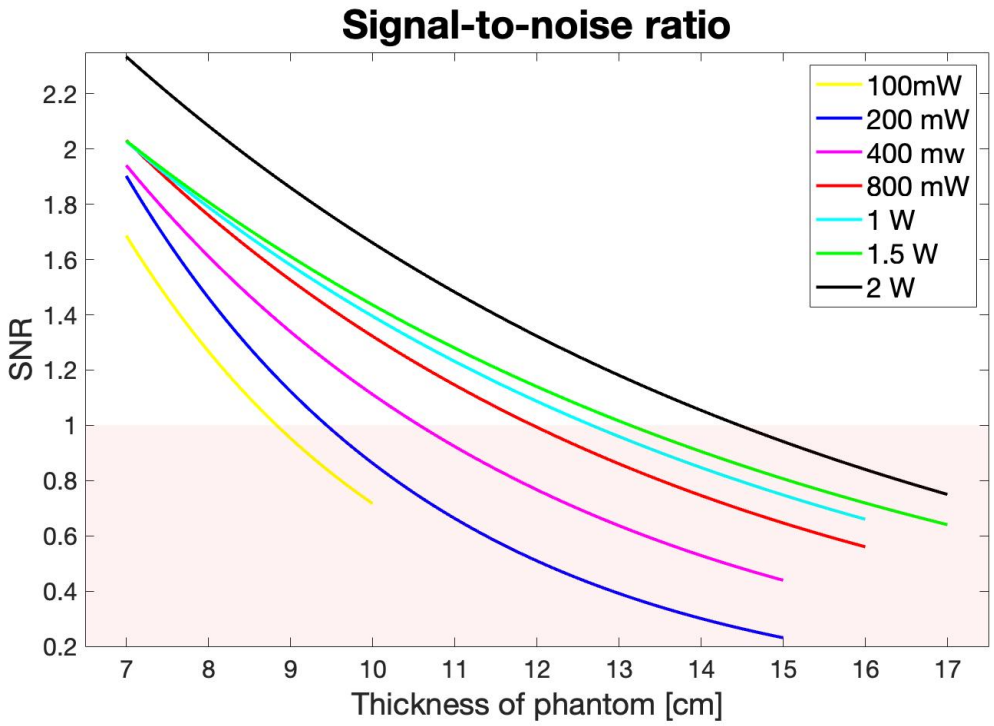

Figure 4.8: Graph showing the fitted curves for each of the powers measured on. The curves are fitted after SNR values shown in table 4.1, values at 12 cm and 13 cm excluded for all. The pink area marks the area below 1, where the SNR is considered too low to get a clear signal.

When comparing the two graphs in figure 4.7, it can be seen that an exponential fit

is not perfect for the data collected at higher powers, but for the lower powers the exponential fit is the most accurate. This might indicate that more measurements collected on even thicker samples may give a more exponential looking curve for the higher powers as well, or simply that stray light was a bigger problem for the higher power at all times.

In contrast to the measurements on gammon with the simple GASMAS setup, here all powers were measured on one thickness at a time, as it was possible to adjust the power without moving the phantom. This means that all measurements for one tissue thickness should have the same detector position in relation to where the laser light enters the phantom. This also means that for different thicknesses, with the same power, the detector position might have changed, as well as a possibility of a change in the composition of the phantom (more or less fat) due to different pieces used, as well as the light entering the phantom at a new spot. Even though highly visible differences were avoided, internal differences might have been present.

As previously stated, Beer-Lambert law (eq. 2.1) is not fully functional for highly scattering medias in the sense that the path length is unknown due to many scattering events, though it is possible to discern similar behavior from the curves in figure 4.8. On average, doubling the power enables measuring through 1 cm thicker tissue with a SNR > 1. While this is not completely true, based on the collected data, it is a rough approximation of the trend indicating that a limit should be found roughly at 15 cm for 2 W. This is highly possible, as 45mW had it's limit at 8 cm when using the GASMAS system.

Table 4.1: Calculated Signal-to-noise value for each power and thickness of phantom. SNR values < 1.0 marked in red. This is set as a practical detection limit although it is possible to detect lower signals. SNR values excluded from the curve fittings are marked in yellow.

	2 W	**1.5 W**	**1 W**	**800 mW**	**400 mW**	**200 mW**	**100 mW**
7cm	1.7631	1.7606	1.7628	1.7651	1.7598	1.7557	1.6573
8 cm	1.7600	1.7617	1.7480	1.7355	1.6664	1.5798	1.2194
9 cm	1.7526	1.7422	1.7283	1.7039	1.6084	1.2803	1.2383
10 cm	1.6736	1.7427	1.6191	1.5976	1.0997	0.9467	0.4927
11 cm	1.5518	1.4306	1.5305	1.3482	0.9509	0.5165	
12 cm	1.7668	1.7240	1.6017	1.4917	1.1143	0.6544	
13 cm	1.7979	1.7836	1.7155	1.6879	1.4253	0.9544	
14 cm	1.4073	1.2036	1.0458	0.9105	0.5415	0.3024	
15 cm	0.8411	0.5964	0.4104	0.2606	0.1782	0.0376	
16 cm	0.7286	0.4842	0.3298	0.2865			
17 cm	0.6058	0.4143					

The SNR values follow a quite symmetrical development relating to power and phantom thickness. If SNR > 1 is considered a good signal, and SNR < 1 is considered a to

small signal in relation too the induced noise, 14 cm is the limit for 1 , 1.5 W and 2 W all together. Although, this should not be considered a fixed value, as it is only based on one measurement averaged over 1000 measurements. While, SNR for 2 W and 1.5 W at 14 cm are quite a bit higher than 1 W, the SNR value for 1 W at 14 cm is just about one, which likely can diverge up and down, depending on e.g detector placement and composition of the phantom.

4.5 Limitations in the light-transmission measurement

The largest limitation with the presented setup is using gammon as tissue phantom. While being real muscle and fat tissue, it lacks some other properties that can affect the light scattering and absorption. Firstly, it is highly possible the gammon has been pumped with water as no control och criteria on the quality of the gammon was put before doing the tests. Secondly, it lacks blood, which as discussed earlier is a big part of the bulk absorption in tissue. These two properties could be changed by using a different type of meat.

When considering how realistic the model actually is it is important to note that this is a very simple model, and that no qualitative limits can be drawn from the use of gammon as phantom tissue, it can only indicate if further development could be successful.

This is also the case when using the Ti:Sa laser instead of the GASMAS system. The limitations of the present GASMAS system has been identified when measuring on gammon, but the measurements done with the Ti:Sa laser can only provide information on how it is possible a GASMAS system with higher power might behave.

In addition, the limit of SNR = 1 is based on measurements without any special techniques for filtering out noise or improving SNR. It is still possible to see a signal even with an SNR = 0.3 (see graph for 200 mW in figure 4.6c), so if any techniques for filtering away noise, such as WMS, was employed, this could further push the limits for GASMAS measurements.

5 Conclusion and outlook

5.1 Conclusion

The Monte Carlo simulations presented a helpful understanding of the scattering process within biological tissue. While being relatively simple models provided a accurate representation that coincided with the results from the tissue-phantom measurements conducted.

The diode laser measurements on gammon show a limit of 8 cm when measuring in transmission with 45 mW. This corresponds to the limit of 15 cm found for 2 W using the Ti:Sa laser system. This limit found is through a phantom consisting of mostly muscle tissue and some adipose tissue, and is therefore not a fully accurate representation of the human anatomy, where for example refraction between different types of tissue should be considered (as can be seen in the simulations presented in 3.3). These measurements were also done in as much transmission as possible to retrieve comparable results between the phantom sizes. This adds a concern to consider in the future, as on a larger body full transmission will be hard to fulfill.

In conclusion it can be said that, while no quantitative conclusions can be drawn from the work presented in this thesis, it still presents a hopeful outlook towards further investigation in introducing GASMAS as a method for monitoring lung function in larger children and adults.

5.2 Outlook for the future

Further development of the tapered amplifier (or another amplifying system) for the diode laser to enable GASMAS measurements at higher power is encouraged. In addition to this development, larger detectors could be tested and evaluated, as the high scattering disperse the photons, and a larger area of detecting should coincide with more detected photons and thus further improve the detection limit.

To further build upon the work presented in this thesis more realistic models should be tested and evaluated, e.g models containing both bone and blood in addition to muscle and fat.

One possibility for measuring on larger children and adults is to place the light source inside the lungs, and detecting on the chest. This could be done with a optic fiber connected to the tracheal tube, for patients under mechanical ventilation. This of course means a more invasive method, which means that it will have a higher risk, thus more test would need to be employed to evaluate such option. In this case, the scattering would be similar to the more realistic simulations (travelling through

skin only once) and the light would be detected in as much transmission as possible, utilizing the fact that tissue is predominately forward scattering. This would also guarantee that all the detected light have travelled through the lungs and therefore oxygen (if oxygen is present in the lungs).

All measurements presented in this thesis have been done on simple models (food), therefore no ethical review was needed to conduct this thesis. For future development, including conducting test on animals or patient, a more thorough ethical review should be performed.

Bibliography

[1] Mayo Clinic Staff. *Pneumothorax - Diagnosis treatment*. https://www.mayoclinic.org/diseases-conditions/pneumothorax/diagnosis-treatment/drc-20350372. Accessed: 2022-06-03.

[2] Mayo Clinic Staff. *Atelectasis - Diagnosis treatment*. https://www.mayoclinic.org/diseases-conditions/atelectasis/diagnosis-treatment/drc-20369688. Accessed: 2022-06-03.

[3] Emilie Krite Svanberg et al. "Diode laser spectroscopy for non-invasive monitoring of oxygen in the lungs of newborn infants". In: *Pediatric research* 79 (2015), pp. 621–628.

[4] Emilie Krite Svanberg et al. "Changes in pulmonary oxygen content are detectable with laser absorption spectroscopy: proof of concept in newborn piglets". In: *Pediatric Research* 89.4 (2021), pp. 823–829.

[5] Sune Svanberg. "Gas in scattering media absorption spectroscopy – from basic studies to biomedical applications". In: *Laser & Photonics Reviews* 7.5 (2013), pp. 779–796.

[6] Yueyu Lin et al. "Gas in Scattering Media Absorption Spectroscopy on Small and Large Scales Towards the Extension of Lung Spectroscopic Monitoring to Adults". In: *Translational Biophotonics* 3 (Aug. 2021).

[7] Katarina Svanberg and Sune Svanberg. "Monitoring Free Gas In Situ for Medical Diagnostics Using Laser Spectroscopic Techniques". In: July 2015, pp. 307–326.

[8] C. Boudoux. *Fundamentals of Biomedical Optics: From Light Interactions with Cells to Complex Imaging Systems*. Pollux, 2017. ISBN: 9781366451194.

[9] Emilie Krite Svanberg. "Non-invasive optical monitoring of free and bound oxygen in humans". PhD thesis. 2016.

[10] Sergio Fantini and Paola Taroni. "16 - Optical Mammography". In: *Cancer Imaging*. Ed. by M.A. Hayat. San Diego: Academic Press, 2008, pp. 445–453.

[11] Steven L Jacques. "Optical properties of biological tissues: a review". In: *Physics in Medicine and Biology* 58.11 (2013), R37–R61.

[12] Sune Svanberg. *Atomic and Molecular Spectroscopy*. 2003, pp. 46–49. ISBN: 9783540203827.

[13] *HITRANonline*. https://hitran.org/. Accessed: 2022-05-17. Line-by-line simulation done for O_2 and all isotopologues.

[14] Sara Pålsson et al. "Kinetics of the superficial perfusion and temperature in connection with photodynamic therapy of basal cell carcinomas using esterified and non-esterified 5-aminolaevulinic acid". English. In: *British Journal of Dermatology* 148.6 (2003), pp. 1179–1188.

[15] Alexey N. Bashkatov et al. "Optical properties of skin, subcutaneous, and muscle tissues: a review". In: *Journal of Innovative Optical Health Sciences* 04.01 (2011), pp. 9–38.

[16] Bratinnica. *Refractive index*. https://www.britannica.com/science/refractive-index. Accessed: 2022-06-04.

[17] 1177.se Johanna Brydolf. *Så fungerar luftvägar och lungor*. https://www.1177.se/Skane/liv--halsa/sa-fungerar-kroppen/luftvagar-och-lungor/. Accessed: 2022-06-09.

[18] Mayo Clinic Staff. *Pneumothorax - Symptoms causes*. https://www.mayoclinic.org/diseases-conditions/pneumothorax/symptoms-causes/syc-20350367. Accessed: 2022-06-03.

[19] Mayo Clinic Staff. *Atelectasis - Symptoms causes*. https://www.mayoclinic.org/diseases-conditions/atelectasis/symptoms-causes/syc-20369684. Accessed: 2022-06-03.

[20] Märta Lewander et al. "Clinical system for non-invasive in situ monitoring of gases in the human paranasal sinuses". In: *Opt. Express* 17.13 (2009), pp. 10849–10863.

[21] James M. Supplee, Edward A. Whittaker and Wilfried Lenth. "Theoretical description of frequency modulation and wavelengthmodulation spectroscopy". In: *Appl. Opt.* 33.27 (1994), pp. 6294–6302.

[22] Ingrid G. Azevedo et al. "Chest circumference in full-term newborns: how can it be predicted?" In: *BMC Pediatrics* 19.1 (2019), p. 341.

[23] Patrik Lundin et al. "Noninvasive monitoring of gas in the lungs and intestines of newborn infants using diode lasers: Feasibility study". In: *Journal of biomedical optics* 18 (Dec. 2013), p. 127005.

[24] *Multi-scattering*. https://multi-scattering.com/.

[25] Joakim Jönsson. "Multi-Scattering: Computational light transport in turbid media". PhD thesis. Combustion Physics, 2021.

[26] Linxi Shi et al. "Skin thickness measurements using high-resolution flat-panel cone-beam dedicated breast CT a". In: *Medical physics* 40.3 (2013), p. 031913.

[27] Aline Bueno et al. "Muscle thickness of the pectoralis major and rectus abdominis and level of physical activity in chronic hemodialysis patients". In: *Orgão oficial de Sociedades Brasileira e Latino-Americana de Nefrologia* 39 (Dec. 2017), pp. 391–397.

[28] D. A. Boas, C. Pitris and N. Ramanujam. *Handbook of Biomedical Optics*. CRC Press, 2011. ISBN: 9780429189289.

[29] London's Global University. *Resources*. https://www.ucl.ac.uk/medical-physics-biomedical-engineering/research/biomedical-optics-research-laboratory-borl/resources. Accessed: 2022-06-09.

Övervaka syrekoncentrationen i lungor: en möjlighet för säkrare intensivvård

Idag diagnostiseras ofta lungkollaps med hjälp av röntgen- eller ultraljudsundersökning av patientens lungor. En nackdel med båda dessa undersökningar är att de enbart ger en ögonblicksbild av patientens tillstånd. Under COVID-19 pandemin ökade antalet patienter på sjukhusens intensivvårdsavdelningar, och många av dem i ett tillstånd som krävde respiratorbehandling på grund av sänkt lungfunktion. En sidoeffekt av behandling i respirator är risken för att lungkollaps sker. Respiratorn kan inte själv känna av om lungorna överbelastas, och det kan därför skapas ett allt för stort tryck som skadar lungorna. Obehandlat kan en lungkollaps vara livshotande.

En övervakningsmetod som inte förlitar sig på patientens egna förmåga att kommunicera sina krämpor, och som inte heller kräver förflyttning, tunga maskiner eller specialutbildad personal hade både kunnat underlätta för personal och bidra till en säkrare vård.

GASMAS (Gas in Scattering Media Absorption Spectroscopy) är en typ av spektroskopi som utnyttjar att alla ämnen har ett unikt absorptionsmönster av ljus. Med andra ord, varje ämne kommer att absorbera en eller flera specifika våglängder. Detta mönster kan jämföras med människans fingeravtryck och är därmed unikt för ett ämne. Eftersom dessa ”fingeravtryck” är kända, går det att låta ljus av olika våglängder färdas genom ett okänt material, och genom att observera vilka våglängder som absorberas går det att identifiera det okända ämnet.

GASMAS har tidigare visats fungera som en mätmetod för att övervaka syrekoncentrationen i lungorna hos bebisar. Genom simuleringar av fotoners spridning i olika typer av vävnad samt praktiska undersökningar med hjälp av modeller har det påvisats att det finns en chans att skala upp metoden så att den även kan användas på vuxna.

Det är viktigt att mängden laser som används är tillräcklig hög för att lyckas färdas genom all vävnad, detta är en blandning av hud, fett, muskelvävnad och lungvävnad, men också är tillräckligt låg, eller utspridd över tillräckligt stor yta för att inte ge patienten brännskador.

De simuleringar som genomfördes gav en förståelse för hur fotonernas spridning påverkas av olika sammansättning av vävnad och hur spridningsprocessen kan se ut. Modellerna som användes var enkla i sin utformning men gav en träffsäker representation när de jämfördes med mätningar på vävnadsfantomer.

Mätningarna som utförde med en diodlaser visade på en övre gräns på 8 cm vävnad i transmission för 45mW, och mätningarna med en Titanium-Safir laser visade på

en övre gräns på 15 cm i transmission för 2W. De vävnadsfantomer som användes bestod till större delen av muskelvävnad och vatten, och är därmed inte en exakt representation av verkligheten.

Eftersom mätningarna som gjordes utfördes i transmission, är det osäkert huruvida gränsen ser ut för mätningar där ljuskälla och detektor placeras så att ljuset först måste färdas in till lungorna och sedan spridas ut igen för att nå detektorn.

Trots att inga exakta slutsatser kan dras, tyder ändå resultaten på att det värt att fortsätta undersöka möjligheterna för att utveckla och skala upp metoden, för att förhoppningsvis kunna bidra till en bättre vård.